

## JGR Solid Earth

## RESEARCH ARTICLE

10.1029/2018JB017049

## Special Section:

Magnetism in the Geosciences  
- Advances and Perspectives

## Key Points:

- We assess 10 alternative approaches for domain state diagnosis as potential replacements for the much used but ambiguous Day diagram
- We recommend adoption of methods that enable domain state identification of each component in samples with complex magnetic mineral mixtures
- We conclude that magnetization curve analysis and FORCs provide the most diagnostic component-specific domain state identifications

## Correspondence to:

A. P. Roberts,  
andrew.roberts@anu.edu.au

## Citation:

Roberts, A. P., Hu, P., Harrison, R. J., Heslop, D., Muxworthy, A. R., Oda, H., et al. (2019). Domain state diagnosis in rock magnetism: Evaluation of potential alternatives to the Day diagram. *Journal of Geophysical Research: Solid Earth*, 124, 5286–5314. <https://doi.org/10.1029/2018JB017049>

Received 20 NOV 2018

Accepted 8 APR 2019

Accepted article online 17 APR 2019

Published online 4 JUN 2019

# Domain State Diagnosis in Rock Magnetism: Evaluation of Potential Alternatives to the Day Diagram

Andrew P. Roberts<sup>1,2</sup> , Pengxiang Hu<sup>1,2</sup> , Richard J. Harrison<sup>3</sup> , David Heslop<sup>1,2</sup> , Adrian R. Muxworthy<sup>4</sup> , Hirokuni Oda<sup>2</sup> , Tetsuro Sato<sup>2</sup>, Lisa Tauxe<sup>5</sup> , and Xiang Zhao<sup>1,2</sup> 

<sup>1</sup>Research School of Earth Sciences, Australian National University, Canberra, Australia, <sup>2</sup>Research Institute of Geology and Geoinformation, Geological Survey of Japan, National Institute of Advanced Industrial Science and Technology (AIST), AIST Tsukuba Central 7, Tsukuba, Japan, <sup>3</sup>Department of Earth Sciences, University of Cambridge, Cambridge, UK, <sup>4</sup>Department of Earth Science and Engineering, Imperial College London, South Kensington Campus, London, UK, <sup>5</sup>Scripps Institution of Oceanography, University of California, San Diego, La Jolla, CA, USA

**Abstract** The Day diagram is used extensively in rock magnetism for domain state diagnosis. It has been shown recently to be fundamentally ambiguous for 10 sets of reasons. This ambiguity highlights the urgency for adopting suitable alternative approaches to identify the domain state of magnetic mineral components in rock magnetic studies. We evaluate 10 potential alternative approaches here and conclude that four have value for identifying data trends, but, like the Day diagram, they are affected by use of bulk parameters that compromise domain state diagnosis in complex samples. Three approaches based on remanence curve and hysteresis loop unmixing, when supervised by independent data to avoid nonuniqueness of solutions, provide valuable component-specific information that can be linked by inference to domain state. Three further approaches based on first-order reversal curve diagrams provide direct domain state diagnosis with varying effectiveness. Environmentally important high-coercivity hematite and goethite are represented with variable effectiveness in the evaluated candidate approaches. These minerals occur predominantly in noninteracting single-domain particle assemblages in paleomagnetic contexts, so domain state diagnosis is more critical for ferrimagnetic minerals. Treating the high-coercivity component separately following normal rock magnetic procedures allows focus on the more vexing problem of diagnosing domain state in ferrimagnetic mineral assemblages. We suggest a move away from nondiagnostic methods based on bulk parameters and adoption of approaches that provide unambiguous component-specific domain state identification, among which various first-order reversal curve-based approaches provide diagnostic information.

## 1. Introduction

Domain state diagnosis is fundamental to paleomagnetic, rock magnetic, and environmental magnetic studies because the distribution of domain states of particles in a magnetic mineral assemblage controls the magnetic properties, including the quality of magnetic recording. The Day diagram (Day et al., 1977) is a biplot (Figure 1a) of the ratio of readily measured hysteresis parameters (the ratios of the saturation remanent magnetization to saturation magnetization [ $M_{rs}/M_s$ ] and the coercivity of remanence to coercivity [ $B_{cr}/B_c$ ], as determined from a major hysteresis loop and a backfield demagnetization curve) and has become a standard tool in rock magnetism for diagnosing magnetic mineral domain states in the stable single-domain (SD) and multidomain (MD) states, and in the intermediate so-called pseudo-single-domain (PSD) state. Most published Day diagrams have data distributions that fall in the PSD region even though the measured magnetic particle systems might not be representative of the PSD state (Roberts et al., 2012; Tauxe et al., 2002). Many difficulties with Day diagram interpretation have long been known. Roberts et al. (2018) recently presented a comprehensive critical appraisal of the Day diagram and pointed to 10 sets of issues that produce uncontrolled unknowns that limit its use for domain state diagnosis, so that hysteresis parameters for single bulk geological samples are usually nonunique in terms of domain state interpretations.

In addition to routine misdiagnosis of domain state from data distributions, widespread use of the Day diagram has contributed to underrecognition of the importance of stable SD particles in the geological record (Roberts et al., 2012) and to reinforcement of the unhelpful PSD concept and of its geological importance

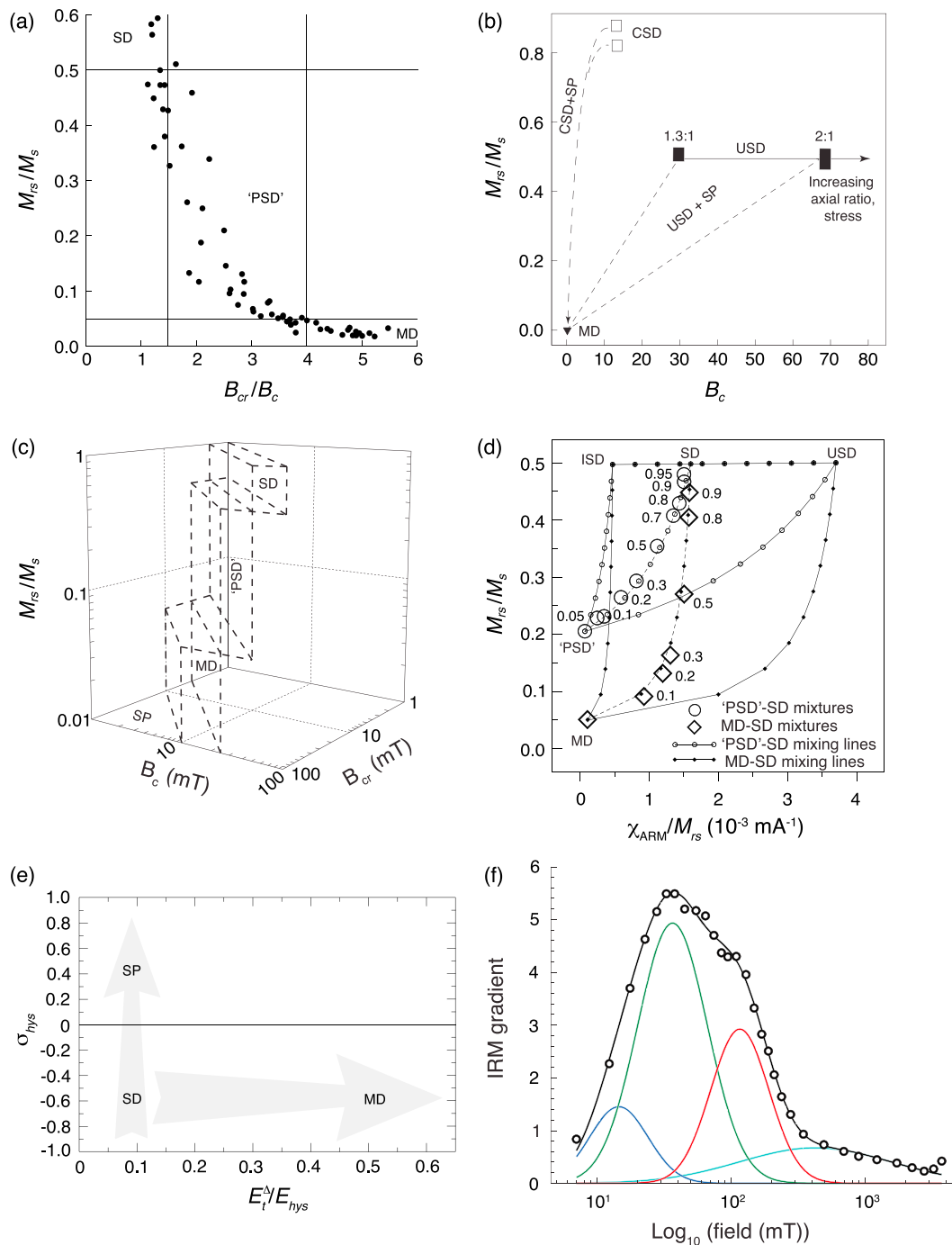


**Figure 1.** Illustration of the domain state diagnosis methods evaluated in this paper. (a) The Day diagram (Day et al., 1977) with regions for SD, PSD, and MD behavior, which has been argued to be fundamentally ambiguous (Roberts, Tauxe, et al., 2018) and for which alternatives must be found. (b) The Néel diagram (Néel, 1955) with a slightly modified interpretive framework provided by Tauxe et al. (2002). See text for explanation, where CSD = cubic single domain, USD = uniaxial single domain, and SP = superparamagnetic. Values in  $M_{rs}/M_s$ — $B_c$  space are shown for magnetite with axial ratios of 1.3:1 and 2:1 from Tauxe et al. (2002). The SP end member must occur at {0, 0}, so the boundaries for USD + SP mixtures have been modified from those of Tauxe et al. (2002). (c) The Borradaile diagram (Borradaile & Hamilton, 2003; Borradaile & Lagroix, 2000) with regions for SD, PSD, and MD behavior. (d) The Lascu diagram (Lascu et al., 2010) with mixing lines for binary mixtures. ISD = interacting SD; USD = as in Figure 1b. (e) The Fabian diagram (Fabian, 2003) with trends for SP admixtures to SD particle assemblages (vertical) and for SD to MD (horizontal) variations (see text for explanation of parameters used in the axes). (f) IRM unmixing for a Chinese loess sample of Eyre (1996) from Heslop (2015). The gradient of the IRM acquisition curve is fitted by log-Gaussian functions to identify four magnetic components.

(Roberts et al., 2017; Tauxe et al., 2002). In this paper, we follow Roberts et al. (2017) in referring to the PSD state as the vortex state (Schabes & Bertram, 1988; Williams & Dunlop, 1989), which includes wide-ranging magnetic behaviors associated with single vortices, multiple vortices, antivortices, cross-tie walls, and Bloch points, although we use PSD when referring to domain state designations used by other authors.

In concluding that the Day diagram is fundamentally ambiguous, Roberts, Tauxe, et al. (2018) stated that its exceptionally wide usage is unlikely to cease unless users are convinced that it is misleading, incorrect, or counterproductively ambiguous. The present paper builds on that work, so we urge readers to engage with this extensive reasoning to understand the necessity of adopting alternative approaches for domain state diagnosis. In recognizing the fundamental ambiguity of the Day diagram, Roberts, Tauxe, et al. (2018) also stated that it is unlikely to be superseded unless suitable alternatives exist. They suggested that adoption of approaches that enable correct domain state diagnosis should be an urgent priority for component-specific understanding of magnetic mineral assemblages and for quantitative rock magnetic interpretation. If domain state can be diagnosed, many of the factors that contribute to ambiguity in the Day diagram become less important because it is the domain state that is being identified rather than variability in other properties.

Alternative approaches to the Day diagram have been proposed in the literature for domain state diagnosis, including the Néel diagram (Néel, 1955; Tauxe et al., 2002); three-dimensional plots with axes  $M_{rs}/M_s$ ,  $B_c$ , and  $B_{cr}$  (Borradaile & Hamilton, 2003; Borradaile & Lagroix, 2000); plots of  $M_{rs}/M_s$  versus  $\chi_{ARM}/M_{rs}$  (Lascu et al., 2010), where  $\chi_{ARM}$  is the susceptibility of anhysteretic remanent magnetization (ARM); plots based on parameters associated with hysteresis loop shape and transient energy dissipation from hysteresis loops (Fabian, 2003); unmixing of isothermal remanent magnetization (IRM) acquisition or backfield demagnetization curves (Heslop et al., 2002; Kruiver et al., 2001; Robertson & France, 1994); alternating field (AF) demagnetization of IRM or ARM curves (Egli, 2004a, 2004b, 2004c); hysteresis loop unmixing (Heslop & Roberts, 2012a; Jackson & Solheid, 2010); first-order reversal curve (FORC) diagrams (Pike et al., 1999; Roberts et al., 2000); remanent, transient, and induced FORC diagrams (Zhao et al., 2017); and unmixing of FORC diagrams by principal component analysis (PCA; Harrison et al., 2018; Lascu et al., 2015). The aim of this paper is to assess such potential candidate approaches to determine their suitability for routine domain state diagnosis in natural magnetic particle assemblages so that practitioners can focus their efforts on use of suitable methods that assist rather than obscure their efforts to interpret magnetic particle assemblages.

## 2. Is Magnetic Domain State Identification a Chimera?

A chimera is something that is hoped for but that is ultimately illusory or impossible to achieve. In a rock magnetic context, it is reasonable to ask whether routine domain state diagnosis is an unachievable ideal. On the one hand, geological samples tend to contain complex magnetic mineral mixtures, so is it possible to identify the domain states of all components in such samples? On the other hand, some materials are encountered relatively routinely in rock magnetism for which the domain state concept is challenging. For example, spin-glass behavior is observed in titanomagnetites and titanohematites, where magnetic spins of constituent atoms are not aligned in a regular pattern (e.g., Ishikawa et al., 1985; Radhakrishnamurty et al., 1981), due to frustration of magnetic exchange interactions. Magnetic domains can be difficult to define across interface boundaries in crystals that contain lamellae or for skeletal crystal forms with irregular shapes (e.g., Harrison et al., 2002; Robinson et al., 2002; Williams et al., 2010). Likewise, identifying the magnetic domain state for some magnetic mineral configurations presents challenges, and contrasting results can be obtained when analyzed with different methods, such as double or multiple magnetosome chain bundles even though individual magnetosome crystals have stable SD properties. Micromagnetic simulations of frustrated systems (Harrison, 2009), particles with complex geometries (Lascu et al., 2018; Williams et al., 2010, 2011), and strongly interacting particle assemblages/magnetofossil chains (Chang et al., 2018; Evans et al., 2006; Harrison & Lascu, 2014; Muxworthy et al., 2003) have improved our theoretical understanding of these issues and are enabling more nuanced interpretations of domain states, which takes us beyond the simple SD-PSD-MD designation. These challenges should be grappled with when relevant; nevertheless, routine domain state diagnosis of geological materials remains fundamentally important in paleomagnetism and environmental magnetism.

### 3. Candidate Approaches for Domain State Diagnosis

In this paper, we evaluate results from 10 approaches that have been proposed for domain state diagnosis. In section 3, we provide an overview of each method and the physical principles that underpin them. We then present results in section 5 for each approach with assessment of their respective effectiveness for domain state diagnosis.

#### 3.1. The Néel Diagram

The Néel diagram, as referred to here, was first used by Néel (1955) and is similar to the Day diagram, but it is a simpler plot of  $M_{rs}/M_s$  versus  $B_c$  rather than  $M_{rs}/M_s$  versus  $B_{cr}/B_c$ . We use the name Néel diagram here to attribute its origin to Néel (1955); it is distinct from diagrams of grain volume versus microscopic coercive force that Dunlop and Özdemir (1997) also referred to as a Néel diagram. Néel (1955) established that  $B_c$  varies with magnetic particle size because the internal demagnetizing field  $-NM$  increases with size, where  $N$  is the demagnetizing factor and  $M_{rs} = B_c/N$  in MD particles. Thus, Néel (1955) used a plot of  $M_{rs}/M_s$  versus  $B_c$  to illustrate particle size trends for coarse geological ferrimagnetic particles. The rationale for use of  $M_{rs}/M_s$  on the vertical axis of the Néel diagram is as follows.  $M_s$  is a material constant for a magnetic mineral and provides a measure of its concentration, whereas  $M_{rs}$  provides a measure of the maximum remanence a magnetic particle can carry, although it is also influenced by the magnetic anisotropy type, including magnetocrystalline and shape anisotropy, stress, and thermal fluctuations. For populations of stable SD particles,  $M_{rs}$  has relatively high values with respect to an applied field direction, whereas  $M_{rs}$  is low for MD particles because significant internal cancellation of magnetic moments occurs due to development of domain structures. Thus,  $M_{rs}/M_s$  is sensitive to magnetic domain state variations (e.g., Dunlop, 1986; Dunlop & Argyle, 1997; Dunlop & Özdemir, 1997; Hunt et al., 1995; Néel, 1955).  $B_c$  and  $B_{cr}$  are also both sensitive to domain state variations when particles are larger (or smaller) than the stable SD threshold size (e.g., Dunlop & Özdemir, 1997; Heider et al., 1996; Hunt et al., 1995; Maher, 1988; Nagata, 1961). Particle size dependence of both  $B_{cr}$  and  $B_c$  can mask important coercivity information associated with different magnetocrystalline anisotropy types when using  $B_{cr}/B_c$ , so Tauxe et al. (2002) preferred plots of  $M_{rs}/M_s$  versus  $B_c$  to Day diagrams. Wang and van der Voo (2004) showed that the Néel diagram provides clear discrimination of coercivity differences between  $\text{Fe}_{2.4}\text{Ti}_{0.6}\text{O}_4$  (TM60) and low-Ti magnetite that is obscured in the Day diagram. Micromagnetic simulations provide valuable constraints on hysteresis interpretation (Muxworthy et al., 2003; Newell & Merrill, 2000; Tauxe et al., 2002; Williams & Dunlop, 1995), but  $B_{cr}$  is often not determined in these simulations. The use of the Néel diagram avoids this requirement and the complexities associated with estimating  $B_{cr}$  from hysteresis results (e.g., Fabian & von Dobeneck, 1997; Roberts, Tauxe, et al., 2018; Tauxe et al., 1996).

Based on the above, Tauxe et al. (2002) suggested that the Néel diagram provides superior domain state diagnosticity than the Day diagram. Using known literature parameters and calculated values, Tauxe et al. (2002) developed a framework to guide interpretation of data variations in  $M_{rs}/M_s$ – $B_c$  space. A  $M_{rs}/M_s = 0.5$  limit is used for uniaxial SD (USD) particles (Stoner & Wohlfarth, 1948). Coercivity increases with particle axial ratio (length/width) in USD materials, so Tauxe et al. (2002) calculated the coercivity of magnetite particles with axial ratios of 1.3:1 and 2:1 (Figure 1b) using predictions from Stoner and Wohlfarth (1948). Intraparticle stress also increases coercivity, as indicated in Figure 1b. Uniaxial anisotropy is not the only important magnetic anisotropy type (Roberts, Tauxe, et al., 2018; Tauxe et al., 2002); many geologically important magnetic minerals have multiaxial anisotropy, so these possibilities should also be considered when representing domain state variability. Open squares labeled CSD are shown in Figure 1b to indicate ideal values for thermally stable cubic SD magnetite particles as predicted by Joffe and Heuberger (1974). Such high  $M_{rs}/M_s$  values are unlikely to occur at room temperature, but higher  $M_{rs}$  values and lower coercivities of CSD particles help to discriminate them from USD particles (Tauxe et al., 2002), which is obscured by use of  $B_{cr}/B_c$  on the horizontal axis of the Day diagram. Expected MD values of  $M_{rs}/M_s$  and  $B_c$  are from Dunlop and Özdemir (1997). Addition of SP contributions to a CSD component is shown following Walker et al. (1993), and a USD + SP region is indicated in Figure 1b from Tauxe et al. (1996). This region should extend to {0, 0} for SP particles and is drawn accordingly in this paper. Néel (1955) plotted data along a similar line from the origin as that for USD particles with axial ratio of 1.3:1 to indicate particle size coarsening toward the origin of the diagram.



Based on the above description, data distributions in regions of the Néel diagram have clear analytical explanations for single magnetic mineral components; however, data for geological and synthetic samples fall in other large regions that have no theoretical explanation. Tauxe et al. (2002) argued that limitations in what can be determined from analytical theory require the use of micromagnetic simulations to explain data distributions in other regions of the Néel diagram. Such results complicate interpretation of simple biplots such as the Néel diagram. Nevertheless, we evaluate the Néel diagram for domain state diagnosis in section 5 below.

### 3.2. The Borradaile Diagram

Borradaile and Lacroix (2000) proposed a diagram with a three-dimensional representation of hysteresis parameters with axes of  $M_{rs}/M_s$ ,  $B_c$ , and  $B_{cr}$  on logarithmic scales (Figure 1c), which we refer to as the Borradaile diagram. Borradaile and Lacroix (2000) and Borradaile and Hamilton (2003) emphasized magnetic discrimination and characterization among different limestone types while maintaining the approach of Day et al. (1977) by designating regions for SD, PSD, and MD particles, along with a region characteristic of SP behavior. The rationale for use of the parameter spaces associated with the Day diagram are described above for  $M_{rs}/M_s$  and  $B_c$ . Plotting of  $B_{cr}$  along a third axis provides an additional dimension for visualizing data variability with a particle-size-sensitive parameter. Overall designation of spaces for respective domain states in the Borradaile diagram follows the trends of  $M_{rs}/M_s$  and  $B_{cr}/B_c$  ratios for domain state boundaries from Day et al. (1977). The Borradaile diagram has not been used widely, but it is worth considering among the other candidate approaches discussed here.

### 3.3. The Lascu Diagram

Lascu et al. (2010) proposed a plot of  $M_{rs}/M_s$  versus  $\chi_{ARM}/M_{rs}$  (Figure 1d) to estimate total ferrimagnetic particle concentration, particle size (domain state) variations, and interparticle magnetostatic interactions in sediments.  $M_s$  is used to estimate ferrimagnetic mineral concentration,  $M_{rs}/M_s$  is a proxy for particle size, and  $\chi_{ARM}/M_{rs}$  is used to estimate interactions. A separate measure of the ratio of the ferrimagnetic susceptibility to  $M_s$  ( $\chi_f/M_s$ ) was used by Lascu et al. (2010) to calculate SP particle contents. Following the use of mixing lines in the Day diagram (Dunlop, 2002), Lascu et al. (2010) calculated binary mixing lines for MD-SD and PSD-SD end-members. They tested this approach with mixtures of known end-members and presented case studies to indicate the value of these often measured bulk magnetic parameters to quantify mass fractions of ferrimagnetic minerals in different domain states. The  $M_{rs}/M_s$  versus  $\chi_{ARM}/M_{rs}$  space (Figure 1d) is interpreted in terms of increasing interactions to the left and coarsening of particle size from top to bottom for the SD (top) to PSD (middle) to MD (bottom) states.

### 3.4. The Fabian Diagram

Fabian (2003) proposed a plot of hysteresis parameters associated with loop shape and transient energy dissipation to provide domain state relevant information that was aimed at enhancing information provided by the Day diagram. The parameters used for the diagram axes are described as follows. The area between the upper and lower branches of a hysteresis loop is the total hysteresis area,  $E_{hys}$ . For undistorted loops,  $E_{hys}$  is given by  $2B_c \times 2M_s$  (i.e.,  $4B_c M_s$ ). Wasp-waisted hysteresis loops have  $E_{hys} > 4B_c M_s$ , and potbellied loops have  $E_{hys} < 4B_c M_s$ . Thus, the parameter  $\sigma_{hys} = \ln\left(\frac{E_{hys}}{4M_s B_c}\right)$  was used by Fabian (2003) as an indicator of SP particles or to indicate the presence of another mineral fraction with contrasting coercivity that can distort hysteresis loop shape (e.g., Jackson, 1990; Roberts et al., 1995; Tauxe et al., 1996). Transient energy dissipation,  $E_t^\Delta$ , as discussed in section 3.9, is represented by the area between a downward branch of a major hysteresis loop and a so-called zero-FORC (Yu & Tauxe, 2005), which is a magnetization curve measured from saturation remanence (i.e., at  $B = 0$ ) back to a saturating field (Fabian & von Dobeneck, 1997). This difference between the upper major loop branch and a zero-FORC is due to irreversible self-demagnetization processes such as domain wall nucleation and pinning (Fabian, 2003) and vortex nucleation and annihilation (Roberts et al., 2017; Zhao et al., 2017). The vertical and horizontal axes in a Fabian diagram are given by  $\sigma_{hys}$  and  $E_t^\Delta/E_{hys}$ , respectively (Figure 1e). Vertical movement from bottom to top is taken to indicate increasing SP particle contents, while movement from left to right represents increasing self-demagnetization in the trend from dominantly SD to MD particles, although no cutoff values are given for particular domain states so that variations are used more in a relative than an absolute sense.

### 3.5. IRM Acquisition or Backfield Curve Unmixing

IRM acquisition or AF/direct current (DC) demagnetization curves provide measures of the coercivity distributions of magnetic particle assemblages. When the first derivative of such curves is taken, observed variability cannot generally be described by a single component (e.g., Figure 1f). Decomposition of such curves into magnetic components (Heslop et al., 2002; Kruiver et al., 2001; Robertson & France, 1994) has become a popular way to understand magnetic mineral assemblages and has contributed significantly to routine recognition of multiple magnetic components in natural samples. To facilitate IRM curve analysis, logarithmically spaced field steps are used to impart an IRM so that many measurements are made at low applied field values and progressively fewer measurements are made at higher fields (e.g., Egli, 2004a; Kruiver et al., 2001). The use of cumulative log-Gaussian (CLG) functions for fitting has become dominant since Kruiver et al. (2001). A log-Gaussian distribution becomes Gaussian when plotted on a logarithmic scale, and properties of CLG distributions are quantified into coercivity-related parameters that are used to interpret coercivity distributions, the magnetization of each component, and its relative contribution to the total magnetization of a sample (Robertson & France, 1994). This information is then used to make inferences about different magnetic mineral and particle size contributions to the total magnetization. Domain state is diagnosed indirectly by comparison of coercivity ranges and coercivity distribution widths (dispersion), where the components of Egli (2004a, 2004b, 2004c) are generally used for magnetite and higher coercivity components are associated, depending on coercivity values, with hematite or goethite. Dispersion is controlled by multiple factors, including particle size, shape, and oxidation distributions, which can create ambiguity in relating coercivity ranges to domain states.

Robertson and France (1994) reported that even single-mineral samples could not be fitted with log-Gaussian functions despite the limited nature of their sample set. The error introduced by such poor fits is unknown when dealing with unconstrained natural magnetic particle assemblages. Egli (2003) used the theoretical model of Egli and Lowrie (2002) for AF demagnetization of an ARM and showed that log-Gaussian coercivity distributions for noninteracting stable SD and MD particles cannot be fitted adequately because the distributions are skewed negatively. Heslop et al. (2004) also observed negative skewing in model results for magnetostatically interacting and thermally activated SD particles. To overcome limitations associated with the negatively skewed distributions that occur widely in natural samples, Egli (2003) showed that better fits are obtained with more flexible skewed generalized Gaussian (SGG) functions. SGG functions have a generalized Gaussian distribution that can have continuously variable skewness and kurtosis (where kurtosis is a measure of the *tailedness* of a probability distribution). SGG fits are defined by parameters that represent the peak of the coercivity distribution ( $\mu$ ), its width ( $\sigma$ ), and magnitude ( $M_{rs}$ ), and by shape parameters  $q$  and  $p$  that describe the distribution's skewness and kurtosis, respectively. Egli (2004b) investigated a range of effects, including particle size, elongation, thermal activation, defects, and surface effects, all of which introduce skewness into coercivity distributions, which supports the use of SGG rather than CLG distributions for coercivity component analysis. The form of SGG distributions has no physical meaning (Egli, 2004b); it is purely a mathematical function that is suitable for fitting coercivity distributions. While better fits are obtained with fewer components using SGG functions, manual fitting of the larger number of parameters is more complicated.

Even though it is well known that SGG functions provide better fits to IRM components, use of CLG fitting remains dominant, presumably because of the ease of use of the Microsoft Excel spreadsheet provided by Kruiver et al. (2001). SGG fitting seems to have fallen into the *expert user* category that has prevented wider uptake. Given the widespread importance of IRM fitting and its evaluation here as an option for routine domain state diagnosis, we point to an illustration from Heslop (2015) who demonstrated a key issue with IRM fitting using CLG and SGG functions. Given that CLG functions cannot fit skewed data, this approach produces fits with more components than those with SGG functions. Heslop (2015) illustrated that CLG fitting produces four components for Swiss atmospheric particulates, whereas a corresponding SGG fit has only two components (Egli, 2004a). In addition to the effects of use of different fitting functions, nonuniqueness of fitted components in IRM analysis is a major weakness of this approach unless semisupervised or supervised unmixing is performed, where independent evidence is used to constrain magnetic component identification and fitting (Heslop, 2015). The stability of SGG fitting can be enhanced considerably by simultaneous fitting of data for sets of samples that contain the same components, as illustrated for complexly mixed samples by Scheidt et al. (2017) using the approach of Egli (2003).

### 3.6. The Egli Diagram

Based on various features associated with AF demagnetization of IRM or ARM curves, Egli (2004a) proposed a diagram with axes of  $\chi_{\text{ARM}}/M_{\text{rs}}$  versus  $\text{MDF}_{\text{ARM}}$  (Figure 2a), which is referred to as the Egli diagram. AF demagnetization characteristics have a long history of use for domain state identification in paleomagnetism and rock magnetism (e.g., Johnson et al., 1975; Lowrie & Fuller, 1971). Like the Day diagram, these approaches are based on the assumption that a single magnetic component is present in natural samples, although Johnson et al. (1975) recognized that a confusing overlap of demagnetization curves occurs when samples contain both fine and coarse magnetic particle fractions. The complexity of typical mixed natural magnetic samples has largely rendered obsolete such tests based on AF demagnetization characteristics. Egli (2004a, 2004b, 2004c) proposed an approach that resolves this issue by using detailed AF demagnetization spectra of ARM and IRM to unmix samples to recognize and characterize multiple magnetic components. ARM and IRM coercivity distributions are obtained by calculating the absolute value of the first derivative of a demagnetization curve. Derivative calculation amplifies measurement noise, which explains the pains taken by Egli (2004a) to minimize demagnetization and/or measurement imprecision or noise. With such measures it can take several days to obtain high-quality data for a single sample. Automated data processing routines can also enable removal of noisy data points (caused, for example, by interference between mains power and the degaussing unit or magnetometer).

As discussed in section 3.4, Egli (2003) introduced SGG functions to provide accurate fits to the shapes of components identified from ARM and IRM acquisition and demagnetization curves. Sediments routinely contain complex mixtures of magnetic components, often with three distinct magnetite components (Egli, 2004a): the biogenic soft (BS) and biogenic hard (BH) components and an undifferentiated component consisting of detrital magnetite and inferred extracellular magnetite (D + EX). Interpretation of these components in terms of domain state is achieved via indirect inference. With the painstaking approach adopted by Egli (2004a) for minimizing the effects of demagnetization and measurement imprecision or noise, fitting errors due to differences between measured and modeled coercivity distributions are generally  $\sim 1\%$  for ARM and less for IRM. The Egli diagram contains regions with different values for the three typical magnetite components (Figure 2a) that occur commonly in sediments. Methods that enable robust unmixing are fundamentally important for extracting paleomagnetic and environmental information carried by individual mineral magnetic components, and the component-by-component specificity of the Egli diagram makes it worth assessing in the present context.

### 3.7. Hysteresis Loop Unmixing

While hysteresis parameters for natural samples provide an ambiguous measure of complexly mixed bulk magnetic properties, hysteresis loop unmixing (Heslop & Roberts, 2012a; Jackson et al., 1990; Roberts et al., 1995; Tauxe et al., 1996) can potentially separate the hysteretic responses of individual components. As discussed in section 3.1, there is an extensive analytical framework for hysteresis loop interpretation when loops represent a single magnetic component. For example,  $M_{\text{rs}}/M_{\text{s}} = 0.5$  is characteristic of USD particles (without thermal activation), whereas higher values are indicative of multiaxial anisotropy. Likewise, MD particle assemblages have low  $M_{\text{rs}}/M_{\text{s}}$  values. In making the case for the presence of vortex states in soft magnetic minerals rather than it being an exotic magnetic state, Roberts et al. (2017) pointed out that loop shapes that are characteristic of individual vortex state particles should not be expected when averaging the response of millions of particles and that these particles will have intermediate hysteresis properties between those of SD and MD end-members. Unmixing of hysteresis loops into separate components (Heslop & Roberts, 2012a) should, thus, provide improved domain state diagnosticity compared to hysteresis parameter interpretation for bulk samples. However, in most data-driven end-member (EM) unmixing approaches, an identified EM can represent a mixture rather than being a magnetically pure single component (Heslop, 2015). The most parsimonious interpretation involves the smallest simplex that encloses all measured data, but the limits of the true unmixing space may be extended beyond this empirically defined space. It can be tempting to extend the boundaries of a mixing space to obtain EMs that represent pure magnetic mineral components; however, environmental or igneous processes often produce mixtures. EM identification can, therefore, be subjective, and parsimonious interpretation is preferable because such solutions are better constrained by data. The key limitation for domain state diagnosticity of hysteresis EMs is the extent to

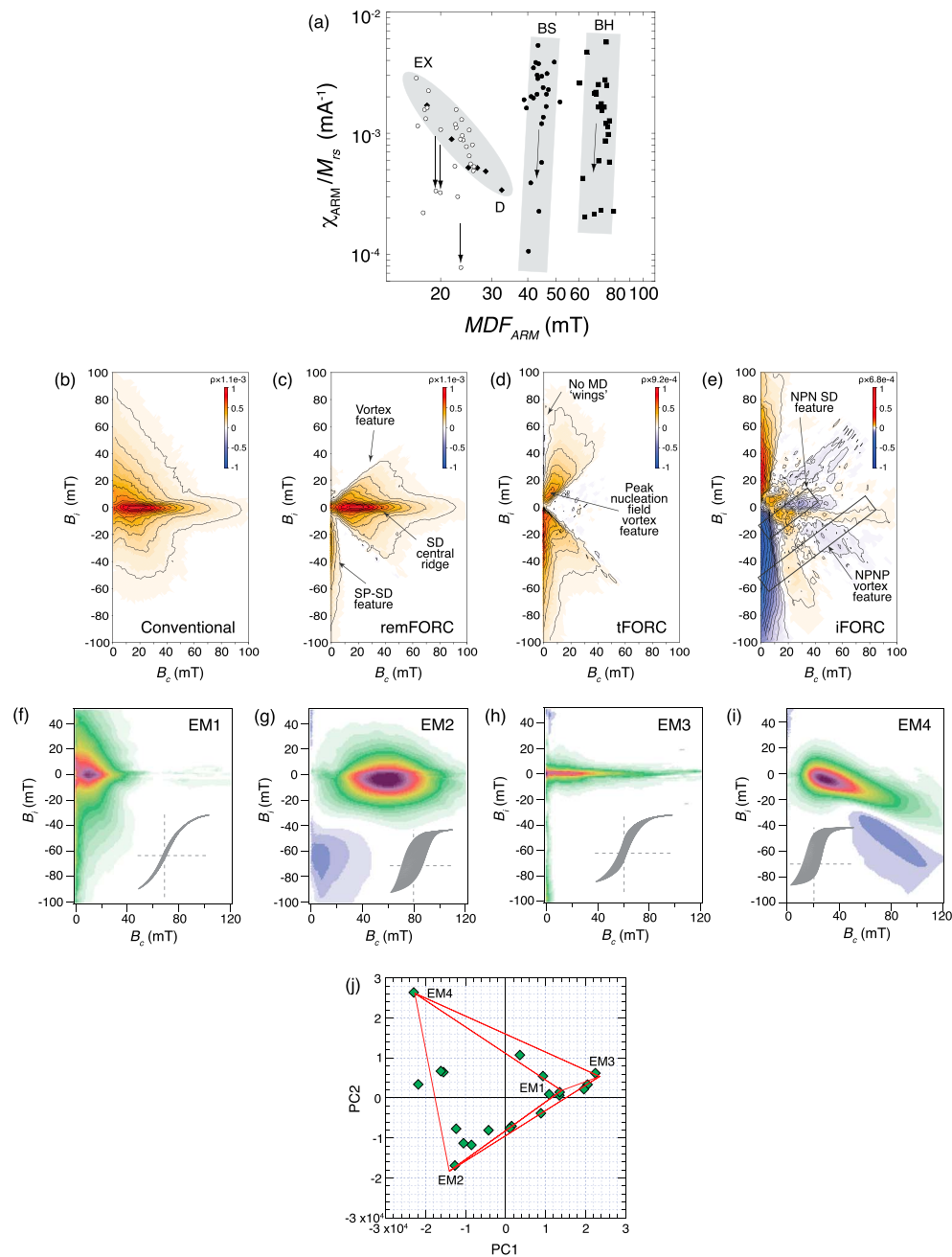


**Figure 2.** Further illustration of the methods evaluated in this paper, particularly FORC-based approaches for domain state diagnosis (Zhao et al., 2017) and FORC unmixing (Harrison et al., 2018). (a) The Egli diagram (Egli, 2004a, 2004b, 2004c) with regions for extracellular (EX), detrital (D), biogenic soft (BS), and biogenic hard (BH) magnetite. The arrows indicate decreasing  $\chi_{ARM}/M_{rs}$  ratios as lake sediments become more anoxic. (b–e) Domain state diagnosis for a clay-carbonate marine sediment from Ocean Drilling Program (ODP) Site 769 (from core 8H-1, 42–44 cm; see Hu et al., 2018, for details). (b) Conventional FORC diagram in which PSD-like (cf. Muxworthy & Dunlop, 2002; Roberts et al., 2000) and noninteracting SD behavior is evident. (c–e) Additional FORC-like diagrams provide a wider diagnostic view of domain states within the sample. (c) A remFORC diagram provides information about remanence-bearing particles, including a noninteracting SD component, a broader contribution from vortex state particles, and a feature along the lower  $B_i$  axis produced by a thermally activated component near the SP/SD threshold (Pike, Roberts, & Verosub, 2001; Zhao et al., 2017). (d) A tFORC diagram, where the upper and lower lobes indicate nucleation/annihilation field distributions for vortex state particles (Roberts et al., 2017; Zhao et al., 2017). (e) An iFORC diagram where induced magnetizations indicate SD (negative-positive-negative, NPN region) and vortex state particles (negative-positive-negative-positive, NPNP region). For interpretive details, see Zhao et al. (2017). (f–j) FORC-PCA unmixing of four magnetic components in sediments from Hydrate Ridge, offshore of Oregon (Larrasoana et al., 2007) that have been subjected to methanogenic diagenesis (Roberts, Zhao, et al., 2018). (f) End member 1 (EM1) is a coarse detrital iron oxide, (g) EM2 is stable SD greigite with strong magnetostatic interactions, (h) EM3 is authigenic SP/SD greigite, and (i) EM4 is authigenic pyrrhotite. A four-component mixing tetrahedron (red lines) is shown in (j) with respect to the two principal components (PC1 and PC2), where green diamonds represent measured FORC data. FORC diagrams in (b–e) were produced with the xFORC software (Zhao et al., 2015), and those in (f–i) were produced with the FORCinel software (Harrison & Feinberg, 2008).

which the EM is a single component. Details of the benefits and limitations of hysteresis unmixing are provided by Heslop and Roberts (2012a).

### 3.8. Conventional FORC Diagrams

FORC diagrams (Pike et al., 1999; Roberts et al., 2000) are based on a class of partial magnetic hysteresis curves known as FORCs (Mayergoyz, 1986). After measuring a series of FORCs within the bounds of a major hysteresis loop, followed by calculation of the second derivative of gridded magnetization measurements, magnetization switching events are mapped in a FORC diagram (e.g., Figure 2b). The Preisach (1935)-Néel (1954) model provides a framework for interpreting responses due to USD particles, where the vertical  $B_i$  axis represents magnetostatic interactions and the horizontal  $B_c$  axis represents coercivity. This picture becomes more complicated for vortex and MD particles because magnetization processes produce different responses for such particles. The horizontal axis for particles in these domain states still provides an approximation of the coercivity, but the vertical axis no longer provides a map of magnetostatic interactions among particles. Instead, for vortex state particles, vertical distributions provide a measure of vortex nucleation and annihilation fields (Pike & Fernandez, 1999; Roberts et al., 2017), and for MD particles, vertical distributions provide a measure of domain wall interactions (Pike et al., 2001). Particles near the SP/SD threshold size commonly give rise to a secondary peak near the origin of the FORC diagram with a dominant vertical response near the  $B_i$  axis in the lower FORC half-plane (e.g., Figure 2c; Pike et al., 2001). In addition to providing information about domain state, Harrison and Lascu (2014) demonstrated that FORC diagrams provide information about the type of magnetocrystalline anisotropy within magnetic particles, which provides further valuable information. Details concerning FORC diagrams and the manifestations of each domain state are provided by Roberts et al. (2014). FORC diagrams have become a standard approach in rock magnetism because they provide direct mapping of microscopic magnetization processes as they relate to domain state in  $B_i$ – $B_c$  space.

### 3.9. Remanent, Transient, and Induced FORC Diagrams

While conventional FORC diagrams have many advantages, Zhao et al. (2017) recognized that they represent a convolution of remanent, induced, and transient magnetizations and that these components can be separated by additional measurement sequences. Measurement details are provided by Zhao et al. (2017) and involve a sequence of conventional FORC measurements, followed by a remanence measurement after each applied field step to enable calculation of a remanent FORC (remFORC) diagram, followed by a return from zero applied field to positive saturation to measure the transient-free magnetization (along a zero-FORC; Yu & Tauxe, 2005), which is subtracted from the downward measured hysteresis loop to obtain the transient magnetization of Fabian (2003) at each field step. Transient magnetizations are then used to calculate a transient FORC (tFORC) diagram. The remFORC diagram provides a valuable measure of the properties of the remanence-bearing magnetic fraction, which is of most interest in paleomagnetism, while the tFORC diagram provides a measure of the distribution of particles with transient hysteresis behavior, which is exhibited dominantly by particles in the vortex and MD states (Fabian, 2003). These two particle types have different manifestations in tFORC diagrams and are readily distinguished from each other (Hu et al., 2018; Roberts et al., 2017; Zhao et al., 2017). Induced magnetizations can also be identified by subtraction of remanent FORC measurements from conventional in-field FORC measurements (Zhao et al., 2017). The resulting induced FORC (iFORC) diagrams provide further valuable information about domain state.

Domain state diagnostic information obtainable from the additional FORC measurements of Zhao et al. (2017) is illustrated in Figures 2b–2e. A conventional FORC diagram is shown in Figure 2b from Hu et al. (2018) for a clay-carbonate marine sediment with typical PSD-like properties (Muxworthy & Dunlop, 2002; Roberts et al., 2000). A noninteracting stable SD contribution would also be inferred from the conventional FORC diagram (Figure 2b). The respective remFORC (Figure 2c), tFORC (Figure 2d), and iFORC (Figure 2e) diagrams provide a clearer view of the magnetic components in this sample. In the remFORC diagram (Figure 2c), in addition to a noninteracting SD *central-ridge*-like signature and a wider remanence-bearing distribution due to vortex state particles, the vertical feature along the lower  $B_i$  axis reflects thermal activation of particles that span the SP/SD threshold (Pike, Roberts, & Verosub, 2001; Zhao et al., 2017). This latter component is not evident in the conventional FORC diagram (Figure 2b) but is observed in almost all but the coarsest of natural samples in remFORC diagrams (Hu et al., 2018; Zhao et al., 2017). Dominant features in the tFORC diagram (Figure 2d) are the upper and lower lobes



that close about a peak at low  $\{B_i, B_c\}$  values that reflect nucleation/annihilation field distributions associated with vortex state particles (Roberts et al., 2017; Zhao et al., 2017). A full understanding of iFORC diagrams has yet to be developed, but Zhao et al. (2017) demonstrated that induced magnetization patterns can be indicative of domain state. For example, the indicated negative-positive-negative-positive (NPNP) feature at larger  $\{B_i, B_c\}$  values (Figure 2e) is associated with vortex state particles, while the negative-positive-negative (NPN) feature at lower  $\{B_i, B_c\}$  values is associated with SD particles. Overall, these additional FORC-like diagrams provide evidence of thermally activated particles near the SP/SD threshold and noninteracting stable SD and vortex state particles with readily diagnosable patterns in each diagram. Collectively, this set of FORC-like diagrams provides substantial domain state diagnostic information that is more clearly discernible than in conventional FORC diagrams. Thus, while remFORC, tFORC, and iFORC diagrams are a type of FORC diagram, we distinguish them from conventional FORC diagrams because of their powerful additional diagnosticity.

It is important to note that tFORC diagrams provide information about magnetic vortices with variable origins. These include vortices that form within single particles due to micromagnetic energy minimization and supervortices that originate from magnetic interactions in composite particles with exsolution lamellae (e.g., Harrison et al., 2002) or through magnetic flux linking among interacting SD particles such as those that form when magnetosome chains collapse (Egli & Winklhofer, 2014; Harrison & Lascu, 2014). These vortex types are all of interest in rock magnetism; distinguishing between them requires detailed microscopic investigations. Hu et al. (2018) presented tFORC diagrams for diverse Australian soils in which magnetofossils are not expected and reported that vortex states occur in all but the coarsest materials (where only MD particles are observed). Thus, despite potential complications due to discriminating vortex from supervortex magnetic structures, tFORC diagrams provide valuable information about domain states in coarse magnetic particles that are less clearly visualized in conventional FORC diagrams.

### 3.10. FORC Unmixing

A key motivation in developing FORC diagrams in rock magnetism was to enable magnetic component identification in complex natural samples (Roberts et al., 2000). While unmixing of the noninteracting USD component was achieved by Egli et al. (2010) and Heslop et al. (2014), Lascu et al. (2015) used PCA to unmix FORC distributions for significant sample sets using processed FORC diagrams. FORC diagrams represent the response of irreversible hysteresis processes, so that they underrepresent magnetizations from particles with weak irreversible magnetizations (e.g., MD and SP particles). Harrison et al. (2018) developed an improved approach by performing PCA on local polynomial regression coefficients rather than on raw FORCs, which provides consistent representation of reversible and irreversible components to enable unbiased quantification of MD and SP contributions. They also developed feasibility metrics to guide users to obtain physically reasonable unmixing results.

Elements of subjectivity exist with PCA unmixing because identified EMs often represent mixtures (Heslop, 2015) and because there is flexibility in placement of EMs. The feasibility metrics of Harrison et al. (2018) provide a visual guide for EM selection to keep users from straying into regions where FORCs cross each other or where they become nonmonotonic. An example of the power of the new FORC-PCA approach for understanding magnetic responses to diagenetic processes is provided by Roberts, Zhao, et al. (2018). The FORC-PCA approach is illustrated in Figure 2f–2j for unmixing of a four-component data set that is representative of methanogenic diagenesis (Roberts, Zhao, et al., 2018). The four components are evident in the tetrahedron that captures variability between the first two principal components (PCs; Figure 2j), where EM1 is a coarse detrital iron oxide component, EM2 is stable SD greigite with strong magnetostatic interactions, EM3 is an authigenic SP/SD component, and EM4 is authigenic pyrrhotite. A key benefit of FORC-PCA unmixing is that it can help users to identify the range of domain states present in a suite of samples, which can be challenging when using conventional FORC diagrams for complexly mixed individual samples. We, therefore, evaluate FORC unmixing for domain state diagnosis in groups of samples in addition to single-sample FORC-type diagrams.

## 4. Methods

The extended description above provides details of the methods evaluated here. We now outline briefly experimental methods used to acquire the data sets discussed in this paper. ARM parameters are

presented for limited data sets, which were imparted by applying a 50- $\mu$ T DC field with a solenoid while a 100-mT peak AF was applied. ARM measurements were completed before IRM acquisition and backfield demagnetization measurements (used for  $B_{cr}$  determinations), which were obtained prior to hysteresis measurements.  $M_{rs}$ ,  $M_s$ , and  $B_c$  were obtained from hysteresis loops. FORC measurement and processing parameters are reported in the respective figure captions. The remFORC, tFORC, and iFORC measurements of Zhao et al. (2017) were made using an irregular grid scheme and were processed using the xFORC software of Zhao et al. (2015), while FORC-PCA unmixing results were obtained using conventional regular measurement grids. The FORC-PCA algorithm of Harrison et al. (2018) is implemented within the FORCinel software of Harrison and Feinberg (2008), which was used for FORC unmixing. IRM acquisition, backfield demagnetization, hysteresis loop, and FORC measurements were measured with various Princeton Measurements Corporation systems in laboratories around the world. Many of the data sets discussed have been published previously; further details of experimental methods can be found in the references cited in the relevant text below.

## 5. Results

Results are presented below for all domain state diagnosis methods discussed in section 3. For most approaches, we present results from extensive data sets from our past work. In particular, we present results for lake sediment samples from a 102-m sediment core from Butte Valley, northern California, and from an Australian national soil database. Samples from Butte Valley contain a complex mixture of magnetic minerals (Heslop & Roberts, 2012a; Roberts et al., 1996) that is useful for testing and illustrating the approaches assessed here. An extensive mineral magnetic data set also exists for the Australian soil samples, which makes it valuable for assessing approaches proposed for magnetic domain state diagnosis (Hu et al., 2018).

### 5.1. The Néel Diagram

Widespread use of hysteresis data in Day diagrams means that extensive data sets also exist for constructing Néel diagrams. In Figure 3, we compare Day and Néel diagrams for >3,100 sedimentary and igneous samples. Several conclusions can be drawn from these data. First, the often scattered data distributions in Day diagrams (Figures 3e, 3g, and 3i) usually collapse into simpler near-linear trends in the respective Néel diagrams (Figures 3f, 3h, and 3j). This indicates that use of a single coercivity parameter rather than the  $B_{cr}/B_c$  ratio provides a better sense of bulk magnetization variability. As shown below, the  $B_{cr}/B_c$  scatter is due to  $B_{cr}$ . For glaciarmarine sediments from Victoria Land Basin, Antarctica (Figure 3f), a progressive bulk fining from older to younger inferred by Roberts et al. (2013) is evident in the Néel diagram (where the CIROS-1 [lower] core contains the oldest sediment and MSSTS-1 contains the youngest). Second, most of the data fall within the USD + SP region defined by Tauxe et al. (2002). This might be taken to indicate a dominance of uniaxial anisotropies, except for our third observation, which is that data for samples dominated by SD biogenic magnetite (Figures 3a and 3b; Roberts et al., 2012) fall to the left of the USD + SP region. Biogenic magnetite is usually associated with uniaxial anisotropy (e.g., Egli et al., 2010) because of flux linking of magnetic particles into a strongly anisotropic chain arrangement (e.g., Dunin-Borkowski et al., 1998). Such chains have aspect ratios far in excess of the 2:1 ratio indicated on the right-hand side of Figure 1b, yet results for samples dominated by USD biogenic magnetite lie to the left of the USD region in Figure 3b. Why? Tauxe et al. (2002) suggested from micromagnetic model results for single particles that the area to the left of the USD + SP region could be indicative of vortex state particles. FORC diagrams for the samples shown in Figure 3b (Heslop et al., 2014; Roberts et al., 2012) contain a strong central ridge signature associated with magnetostatically noninteracting USD particles (Egli et al., 2010), as well as a more vertically spread component. Heslop et al. (2014) labeled this latter component as the (D + EX) magnetite component of Egli (2004a). If this component is due to vortex states in detrital particles—or to supervortex states in collapsed magnetofossil chains as suggested by Harrison and Lascu (2014) and Egli and Winklhofer (2014)—it could produce magnetic responses that lie to the left of the USD + SP region of the Néel diagram. We do not seek to explain these ambiguities further here. The key point is that ambiguities exist in such data representations based on bulk hysteresis parameters because we lack the specificity associated with component-by-component analysis.

Overall, the Néel diagram has some advantages over the Day diagram. First, it avoids the obscuring effects of the  $B_{cr}/B_c$  ratio, where both  $B_{cr}$  and  $B_c$  are sensitive to particle size variations. In our data sets,  $B_{cr}$  is more

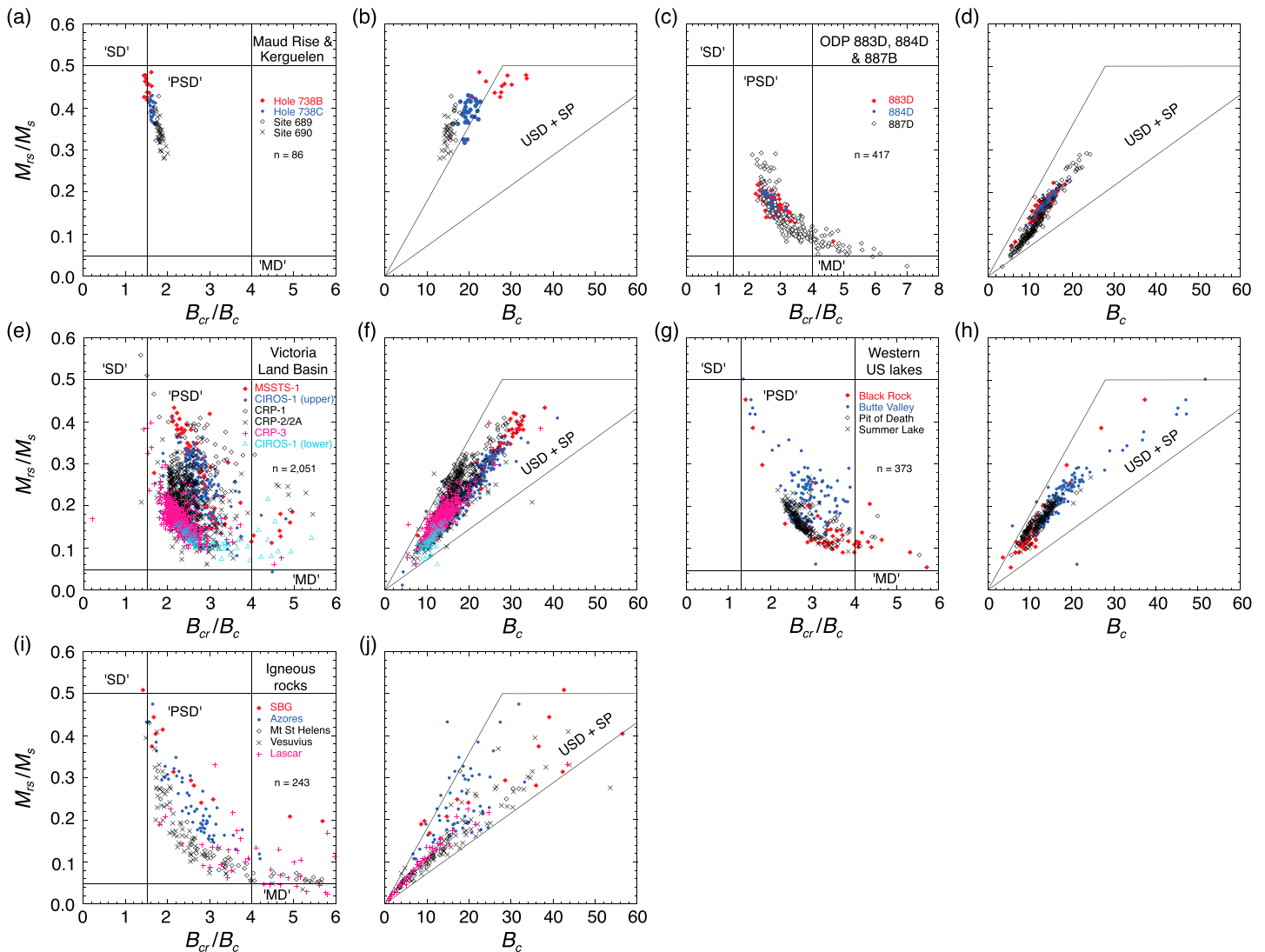


**Figure 3.** Data distributions in Day and Néel diagrams for samples from which comparisons are made with other methods in this paper. (a) Day and (b) Néel diagrams for biogenic marine sediments (pelagic carbonates) from ODP Holes 738B and 738C and Sites 689 and 690. (c) Day and (d) Néel diagrams for terrigenous marine clays from ODP Holes 883D, 884D, and 887D. (e) Day and (f) Néel diagrams for glaciarmarine sediments from Victoria Land Basin, Antarctica. Samples are from (older to younger) the CIROS-1 (lower), CRP-3, CRP-2/2A, CRP-1, CIROS-1 (upper), and MSSTS-1 drill holes. (g) Day and (h) Néel diagrams for lake sediments from the western U.S., including Black Rock, Butte Valley, Pit of Death, and Summer Lake. (i) Day and (j) Néel diagrams for submarine basaltic glass (SBG) and extrusive rocks from the Azores Islands (Portugal), Mt St Helens (USA), Vesuvius (Italy), and Lascar (Chile). Hysteresis results for the various data sets have been discussed previously by Roberts et al. (2012), Roberts, Tauxe, et al., (2018) with citation of source references. The region for USD + SP magnetite (Figure 1b) from Tauxe et al. (2002) is indicated on the respective Néel diagrams.

variable than  $B_c$ , so that  $B_{cr}/B_c$  produces scatter in a Day diagram that is not present in the Néel diagram for the same data (Figure 3). Thus, a reasonable case can be made that the Néel diagram provides a more useful representation of hysteresis data than the Day diagram (see Wang & van der Voo, 2004). Its overall value is discussed more broadly in relation to other methods in section 6.

## 5.2. The Borradaile Diagram

Hysteresis data can also be represented readily in Borradaile diagrams (Figure 4). When visualized along the  $B_{cr}$  axis (not shown), it becomes clear that the large data scatter in the Day diagrams in Figures 3e, 3g, and 3i is due to scatter in  $B_{cr}$ . This scatter is not evident in the respective Néel diagrams, where  $M_{rs}/M_s$  is plotted versus  $B_c$ . This indicates two important things. First, the use of  $B_{cr}$  complicates the Day diagram by adding scatter to it. Second, use of the  $B_{cr}/B_c$  ratio in the Day diagram complicates representation of particle size-

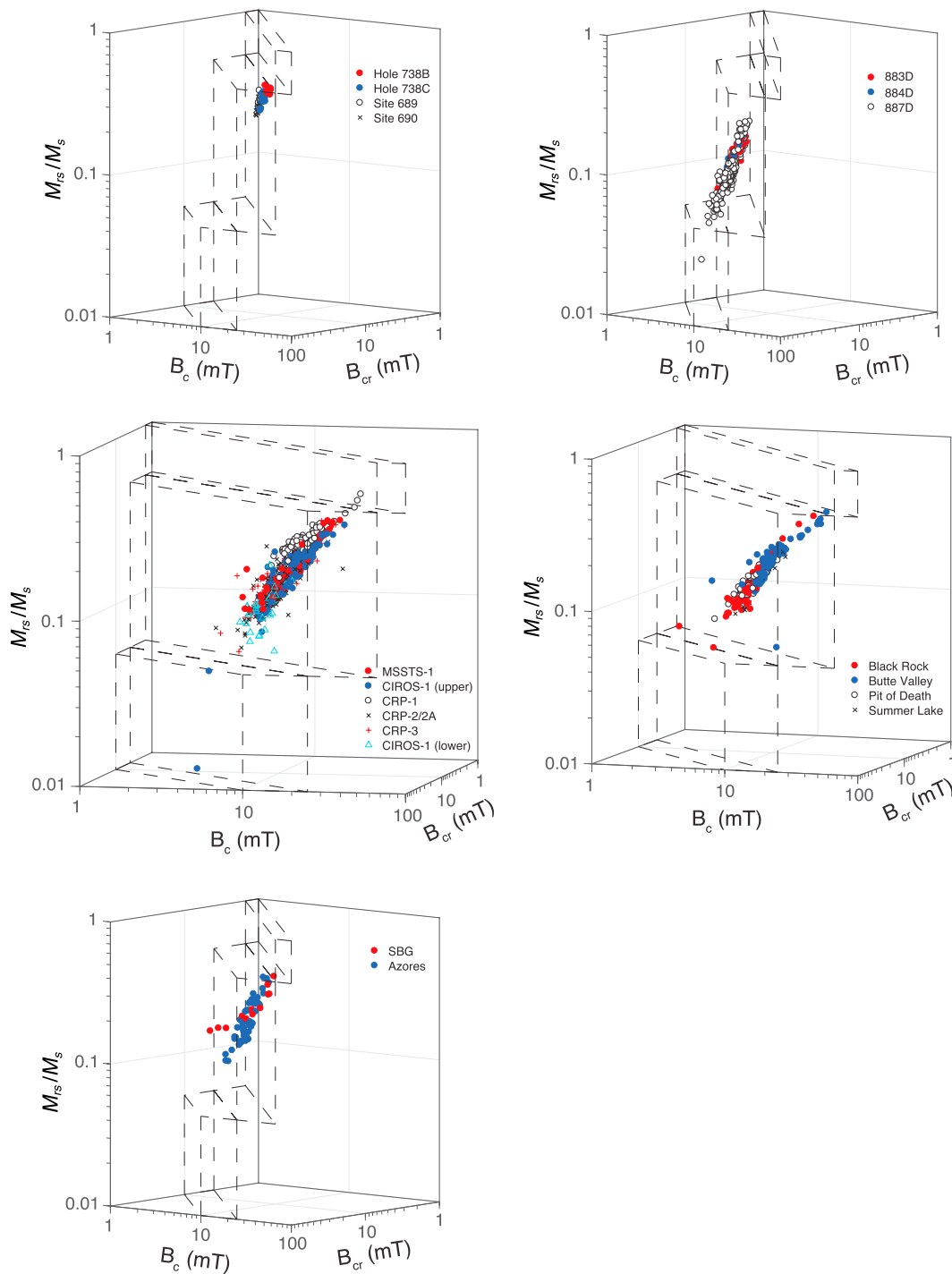


**Figure 4.** Borraidaile diagrams for a subset of locations shown in Figure 3. SD, PSD, and MD regions, as illustrated in Figure 1c, are indicated without labels following Borraidaile and Lagroix (2000) and Borraidaile and Hamilton (2003). The diagrams have been rotated by different (arbitrary) amounts to facilitate visualization of trends in each data set.

related variations by taking a ratio of two parameters that each respond to such variations. Separation of these factors in both the Néel and Borraidaile diagrams makes these lesser used diagrams useful for visualizing data trends. The Borraidaile diagrams in Figure 4 are shown in orientations that aid visualization of principal trends in each data set. This is consistent with the spirit in which these diagrams were proposed, where Borraidaile and Lagroix (2000) and Borraidaile and Hamilton (2003) emphasized

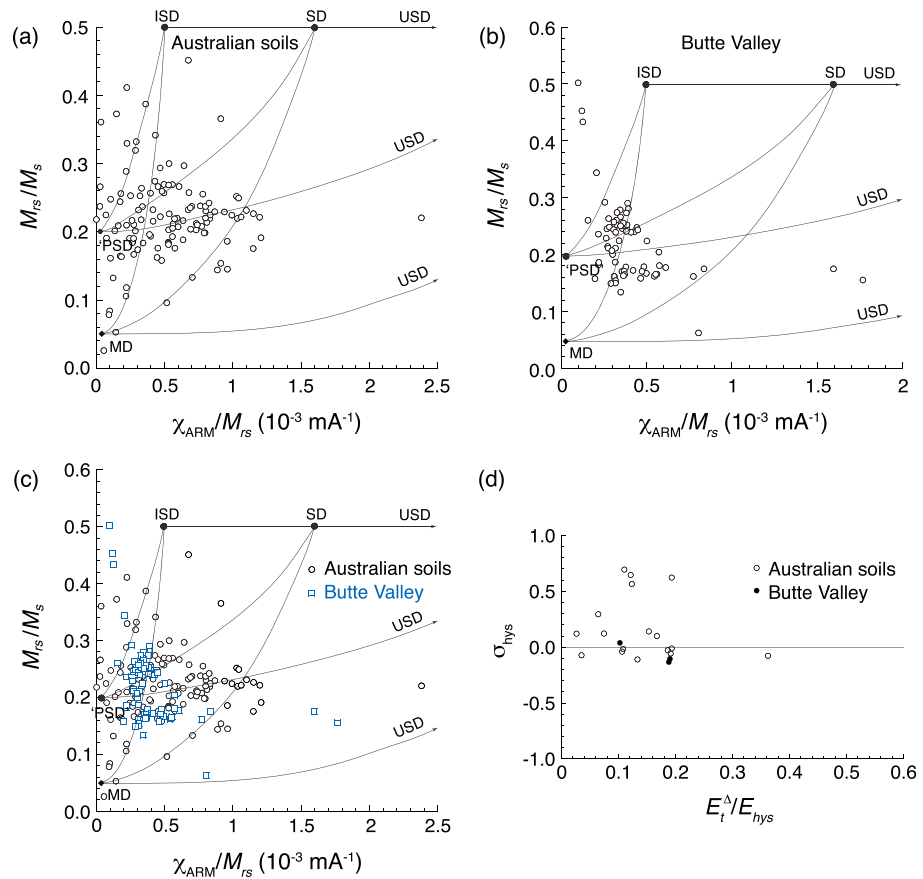


**Figure 5.** Lascu diagrams for samples from (a) the Australian national soil archive (Hu et al., 2018) and (b) lake sediments from Butte Valley, northern California (Roberts et al., 1996). (c) Results from both data sets have overlapping bulk magnetic properties in contrast to the lack of overlap for the same data sets in the Egli diagram in Figure 6. (d) Fabian diagram for a selection of Australian soil and Butte Valley samples. Compared to the data trends indicated in Figure 1f, the data distribution for these samples is indicative of SD and relatively fine vortex state particles with significant SP contents.

their use for characterizing limestone types. Plotting  $B_{cr}$  and  $B_c$  separately has advantages for visualizing data, where changing the diagram orientation interactively on a computer screen is preferable to printing in a fixed orientation. Overall, the major limitation of the Borradaile diagram is the same as for the Day diagram because bulk hysteresis data representations are not component specific. The same regions are used to designate SD, PSD, and MD behavior as in the Day diagram; however, these designations are not linked to particular  $B_c$  and  $B_{cr}$  values, and the boundaries indicated for domain state regions are based on  $M_{rs}/M_s$  and  $B_{cr}/B_c$  ratios rather than  $B_c$  and  $B_{cr}$  values. This means that SD magnetite could have unrealistically low or high  $B_{cr}$  and  $B_c$  values as long as the  $B_{cr}/B_c$  ratio is consistent with SD behavior. We conclude that the Borradaile diagram does not provide a meaningful advantage to the Day diagram for magnetic domain state diagnosis.

### 5.3. The Lascu Diagram

Results are shown in a Lascu diagram in Figures 5a and 5b for Australian soils (Hu et al., 2018) and Butte Valley sediments (Roberts et al., 1996), respectively. By reference to the definitions and mixing lines for the Lascu diagram (Figure 1d), data trends for these sample sets are dominated by low  $M_{rs}/M_s$  values and low  $\chi_{ARM}/M_{rs}$  values (mainly  $< 0.5 \times 10^{-3} \text{ mA}^{-1}$ ) that Lascu et al. (2010) suggested to be associated with coarse, interacting ferrimagnetic particle assemblages. Data scatter is indicative of variable particle size (vertical axis) and variable interactions/anisotropy type (horizontal axis). A dominance of coarse detrital particles is a reasonable overall characterization. Both data sets are plotted together in Figure 5c, which demonstrates their large overlap. As shown below, the Butte Valley data set is complex and contains different magnetic mineral components with variable domain states.



Like other methods discussed above, the Lascu diagram is based on bulk parameters, with the same vertical axis as the Day diagram. It, therefore, suffers from the same major deficiency concerning lack of component-specific domain state diagnosticity. Unlike the methods discussed so far, however, the Lascu diagram was designed for complexly mixed sample sets where the aim is to characterize each component independently and then to unmix large sample sets into potential EMs. This approach is realistic in treating natural samples as complex mixtures that must be understood on a component-specific basis with quantitative determination of the concentration of each component. In reviewing the effectiveness of magnetic unmixing approaches, Heslop (2015) referred to this approach as the current state of the art for supervised unmixing. Thus, even though the Lascu diagram is a plot of bulk parameter values, identification of each magnetic component and quantifying its contribution enables definition of a magnetic mixing space. Thus, the Lascu diagram, when used as it was intended, avoids many of the pitfalls associated with the use of bulk magnetic parameters. It, therefore, has potential for magnetic unmixing, and its efficacy is evaluated below by comparison with other methods.

#### 5.4. The Fabian Diagram

Results are shown in a Fabian diagram in Figure 5d for 20 samples from Australian soils and Butte Valley. Compared to the data trends indicated in Figure 1e, and the examples used by Fabian (2003) to illustrate the method, our data have  $\sigma_{\text{hys}}$  values that are indicative of significant SP particle contents (i.e.,  $\sigma_{\text{hys}}$  is positive or close to zero).  $E_t^\Delta/E_{\text{hys}}$  values are  $<0.2$ , except for one sample, which are indicative of SD to relatively fine vortex state particles. These conclusions are consistent with those discussed below for the Butte Valley samples and with remFORC and tFORC diagrams presented for the Australian soil samples by Hu et al. (2018). The Fabian diagram, therefore, appears to have diagnostic value. However, as stated by Fabian (2003): "... as with  $M_{\text{rs}}/M_{\text{s}}$ , it is neither possible to discriminate mixtures of SD and MD particles from PSD particles by  $E_t^\Delta/E_{\text{hys}}$ , nor ...". He concluded that  $E_t^\Delta/E_{\text{hys}}$  reflects the average *magnetic grain size*. The approach recommended here is to move away from such bulk average parameters and to identify constituent magnetic components within samples. Likewise, lack of specific  $E_t^\Delta/E_{\text{hys}}$  values with respect to the SD, vortex, or MD states is a further limitation of the Fabian diagram. Nevertheless, the concepts of Fabian (2003) have exceptional value with respect to determining transient magnetization distributions, which contribute to domain state identification in the tFORC diagram of Zhao et al. (2017). We discuss the value of the Fabian diagram for domain state diagnosis further below.

#### 5.5. Magnetization Acquisition or Demagnetization Curve Unmixing

Unmixing based on ARM or IRM acquisition/demagnetization seeks by definition to identify components within complex samples, so it avoids the fundamentally limited bulk parameter approaches that provide minimal domain state diagnosticity. Unmixing examples are abundant in the literature, so we only present one example here of a three-EM unmixing analysis using the software of Maxbauer et al. (2016) with SGG functions for AF demagnetization data of ARM and IRM, respectively, for 15 Australian soil samples (Figures 6a and 6b). EM1 is interpreted to represent low-coercivity coarse detrital MD particles. EM2 is interpreted to represent fine, probably pedogenic, magnetite/maghemite, which overlaps the region for pedogenic magnetite defined by Egli (2004a). EM3 is a high-coercivity maghemite/hematite component that is more evident in IRM than in ARM data. This is as expected because hematite will contribute to IRM while not contributing significantly to ARM (Figures 6a and 6b).

The biggest issues with magnetization curve unmixing are the uniqueness of solutions and the type of mathematical function used for component fitting. Heslop (2015) emphasized the need for independent evidence about the nature of components to *supervise* unmixing because unconstrained fitting of magnetic data produces fundamentally nonunique solutions. Extensive magnetic characterization is performed in most rock magnetic studies, and this information is used to constrain unmixing interpretations so that most such attempts are at least semisupervised. The bigger issue concerns the use of CLG versus SGG functions for component fitting, as discussed above. CLG functions have been demonstrated to produce more components than are necessary because natural magnetic particle size (i.e., coercivity) distributions are typically skewed (Egli, 2003; Heslop, 2015). This makes SGGs more suitable, and we recommend their use, but the larger number of fitting parameters makes such fitting more complex so that SGG functions are not used as frequently as they should be. Regardless, we conclude that magnetization curve unmixing, when supervised

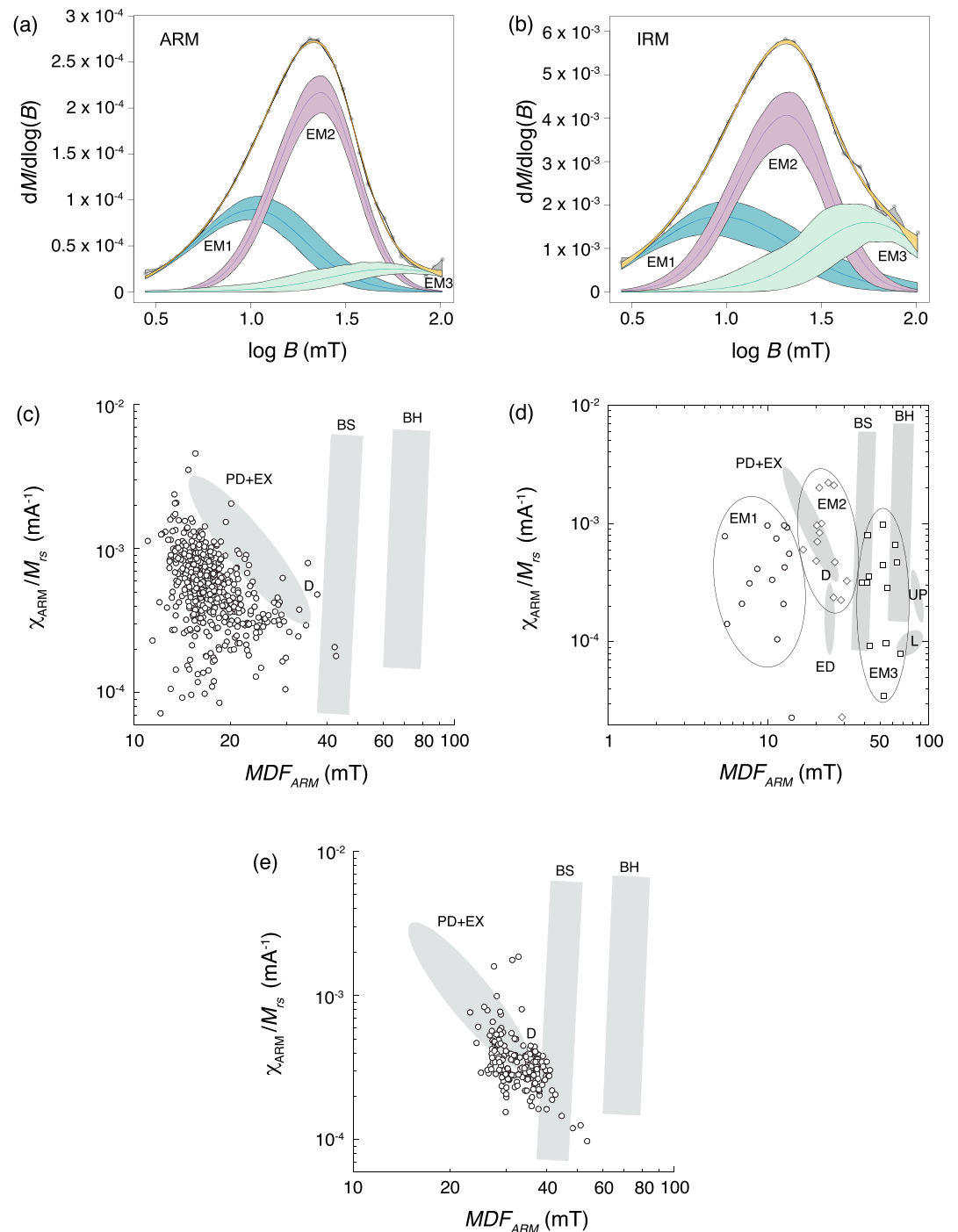


**Figure 6.** Examples of ARM and IRM unmixing and Egli diagrams for samples from (a and b) the Australian national soil archive (Hu et al., 2018) and (e) lake sediments from Butte Valley, northern California (Roberts et al., 1996). (a) ARM and (b) IRM unmixing was done with SGG functions for a subset of 15 Australian soil samples using the software of Maxbauer et al. (2016) from which three EMs are identified. Egli diagrams for (c) bulk data for the entire Australian soil data set of Hu et al. (2018) and (d) for each EM from the subset of 15 samples (see text for discussion). Butte Valley results in (e) are also bulk measurements, which are shown for illustration even though the Egli diagram is designed for individual magnetic components. Ares are labeled from Egli (2004a) for additional magnetic particle types to those shown in Figure 2a: PD = pedogenic magnetite; ED = eolian dust; L = loess; and UP = urban pollution.

with independent data, can be a highly effective method for magnetic component identification. Such analyses do not diagnose the domain state of identified components directly. This association is made by relating the coercivity distribution of a component to those of known magnetic particle types, largely through the work of Egli (2004a, 2004b, 2004c).

### 5.6. The Egli Diagram

Results are shown in Egli diagrams in Figures 6c–6e for Australian soils (Hu et al., 2018) and Butte Valley sediments (Roberts et al., 1996). We only have sufficient data of the type recommended by Egli (2004a, 2004b, 2004c) to follow his approach rigorously for Australian soil samples. While we do not advocate the use of bulk rather than component-specific approaches, we present bulk parameter values in the Egli diagram to illustrate results for these data sets. By reference to regions identified in the Egli diagram for different magnetite types (Figure 2a), Australian soils have low coercivities and bulk data fall dominantly below the D + EX region (Figure 6c). Based on extensive magnetic property evaluation of the studied Australian soils, which are dominantly dry and not water-logged, Hu et al. (2018) argued that no biogenic magnetite is present. This is consistent with data trends in the Egli diagram, where bulk coercivities are too low to be confused with those expected for biogenic magnetite. Lower than expected  $\chi_{\text{ARM}}/M_{\text{rs}}$  values are likely due to the widespread presence of hematite in these soils, as indicated by nonzero *hard* IRM (HIRM) and S-ratio values that are much less than 1 (data not shown here). Hematite will not contribute significantly to  $\chi_{\text{ARM}}$ , but contributes to  $M_{\text{rs}}$ , which produces lower  $\chi_{\text{ARM}}/M_{\text{rs}}$  values than expected for detrital magnetite alone. ARM demagnetization curves for Australian soils were subjected to EM unmixing from which we identify three EMs (Figure 6a). The studied Australian soils are dominated by coarse lithogenic magnetite (EM1) that dominates the bulk magnetic properties. Higher coercivity contributions due to fine pedogenic magnetite (EM2) and maghemite/hematite (EM3) are also identified. The clear distinction of the magnetic properties of the three EMs demonstrates the value of the Egli diagram (Figure 6d).

By contrast to Australian soils, bulk data from Butte Valley sediments (Figure 6e) straddle regions for the D + EX and BS magnetite components of Egli (2004a). FORC diagrams for Butte Valley samples suggest the presence of both detrital and biogenic magnetite (Roberts et al., 2012). So even though bulk measurements do not comply with the measurement requirements of Egli (2004a, 2004b, 2004c), data trends for Butte Valley samples fall within reasonable parts of the Egli diagram that make sense based on other available information. When data of the type specified for the Egli diagram are available, and the requisite acquisition or demagnetization curves are unmixed as specified, magnetic component-specific diagnosticity is achieved (Figure 6d). We conclude, therefore, that the method of Egli (2004a, 2004b, 2004c) is highly suitable for domain state diagnosis via linking of the coercivity properties of identified components to those of the different magnetite types indicated in the Egli diagram. However, we note that although the work of Egli (2004a, 2004b, 2004c) is cited widely in relation to unmixing and to identification of commonly identified component types, relatively few studies have adopted either the proposed rigorous measurement approach or the use of SGGs as advocated for use in the Egli diagram.

### 5.7. Hysteresis Loop Unmixing

Extensive use of hysteresis loops in rock magnetism makes direct unmixing of loops a valuable approach. An example of hysteresis loop unmixing from the Butte Valley sediment core is provided in Figure 7 from Heslop and Roberts (2012a) who used it to demonstrate the method. Heslop and Roberts (2012a) identified three EMs from hysteresis unmixing, where EM1 is a mixture of detrital (titano-)magnetite and hematite derived from the local catchment, EM2 is SP glacial rock flour derived from the catchment, and EM3 is SD greigite that formed authigenically within the sediments (Figures 7a–7c). EM1 consists of a mixture of components as indicated by the wasp-waisted hysteresis loop (Roberts et al., 1995; Tauxe et al., 1996) in Figure 7a. Heslop and Roberts (2012a) interpreted EM3 to be due solely to greigite, which occurs mainly in restricted parts of the Butte Valley core below 90 m and at only two stratigraphic intervals above 20 m (Roberts et al., 1996). The presence of an extensive SD component throughout the core (Figures 7d and 7e), therefore, needs explanation. Roberts et al. (2012) identified that a central ridge signature that is indicative of noninteracting SD particles (Egli et al., 2010) is common in the Butte Valley core (e.g., Figures 8a and 8b). Roberts et al. (2012) interpreted this noninteracting SD signature to be due to biogenic magnetite. Thus, EM3 is likely to be due in some cases to noninteracting SD magnetite and in other cases to interacting SD greigite (e.g., Figure 8e). This ambiguity is due to the nonuniqueness of hysteresis interpretation, which can be resolved by the greater information

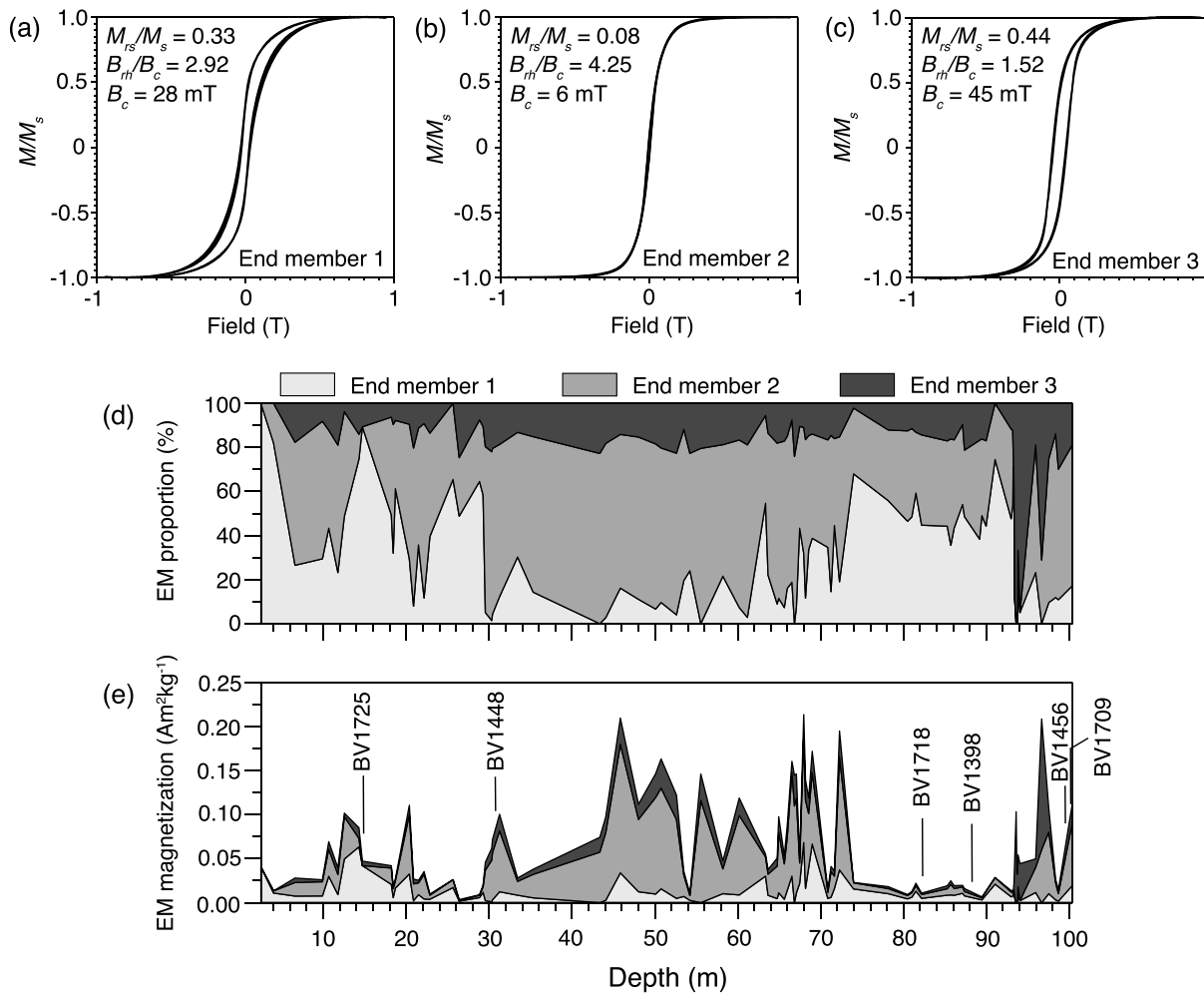


**Figure 7.** Hysteresis unmixing results for samples from Butte Valley, northern California (Roberts et al., 1996). Heslop and Roberts (2012a) identified three magnetic components from hysteresis loop unmixing. The loops in (a–c) represent means of the three EM loops, where the variable line thickness reflects variations in the  $\pm 1$  standard error.  $M_{rs}/M_s$  ratios and  $B_c$  are given for each loop. (a) EM1 is a mixture of detrital (titano-)magnetite and hematite derived from the local catchment, (b) EM2 is SP glacial rock flour derived from the local catchment, and (c) EM3 is authigenic SD greigite and SD biogenic magnetite. An EM may be a mixture, as indicated by the wasp-waisted hysteresis loop in (a) for EM1 (Jackson, 1990; Roberts et al., 1995; Tauxe et al., 1996).  $B_{cr}$  is estimated as the median field of the remanent component of the loop ( $B_{rh}$ ) following Fabian and von Dobeneck (1997), as indicated in the  $B_{rh}/B_c$  ratio (a–c). (d) Relative and (e) absolute abundances of the three EMs for the Butte Valley sediment core with respect to depth. Stratigraphic positions of the six samples for which FORC diagrams are shown in Figure 8 are indicated in (e).

provided by FORC diagrams, where the central ridge signature (Figures 8a and 8b) is distinguishable from that due to interacting SD greigite (Figure 8e). The fact that EMs can represent mixtures requires additional magnetic characterization to facilitate interpretation. Overall, as discussed in section 3.7, a parsimonious mixing space that contains all measured data is preferable without pushing the limits of the mixing simplex toward single-component EMs because natural processes can produce mixed EMs (e.g., EM1). Quantification of relative and absolute abundances of the three Butte Valley EMs downcore (Figures 7d and 7e) enables determination of the contribution of both reversible and irreversible magnetization components. This makes hysteresis unmixing valuable for quantifying stratigraphic variations of EMs in sediment cores, which can then be related to environmental processes. Hysteresis unmixing has yet to be used widely despite the fact that hysteresis loops are measured routinely in rock magnetic studies.

### 5.8. Conventional FORC Diagrams

FORC diagrams for representative Butte Valley samples illustrate the presence of dominantly noninteracting SD magnetite (Figures 8a and 8b), dominantly vortex state magnetite (Figures 8c and 8d), and

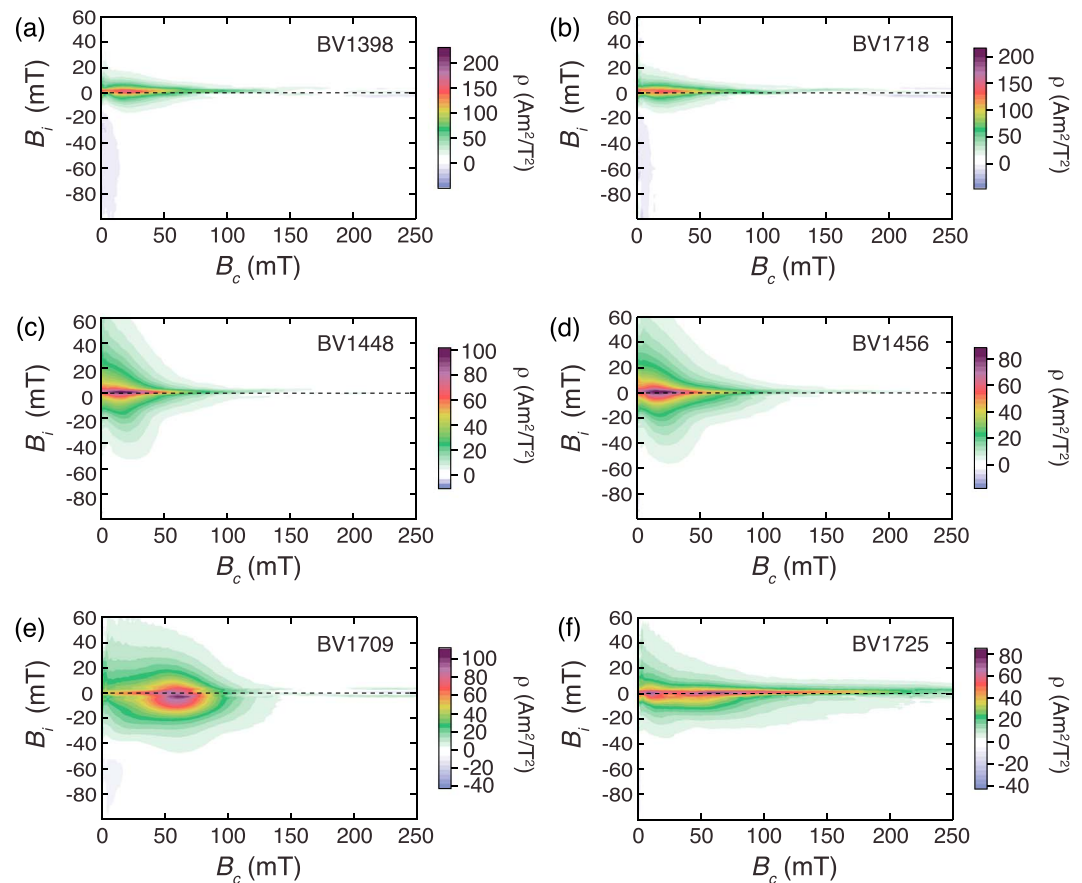


**Figure 8.** Representative FORC diagrams from the Butte Valley sediment core (Roberts et al., 1996). Samples are shown with dominantly noninteracting SD magnetite: (a) BV1398 (88.12 m in the core) and (b) BV1718 (82.23 m); dominantly vortex state magnetite: (c) BV1448 (30.73 m) and (d) BV1456 (99.60 m); interacting SD greigite: (e) BV1709 (100.24 m); and a mixture of vortex state magnetite, moderately interacting greigite, and higher-coercivity hematite: (f) BV1725 (14.47 m). All samples were measured with a regular measurement grid with 200-ms averaging time and were processed with VARIFORC smoothing parameters (see Egli, 2013) of  $s_{c,0} = 3$ ,  $s_{c,1} = 3$ ,  $s_{b,0} = 7$ ,  $s_{b,1} = 7$ , and  $\lambda_c = \lambda_b = 0.1$ .

interacting SD greigite (Figure 8e). Complexly mixed samples contain noninteracting SD and vortex state magnetite and higher-coercivity hematite (Figure 8f). All components identified in Figure 8 have been identified in detailed magnetic characterizations of the Butte Valley core (Roberts et al., 1996, 2012). Ambiguities in hysteresis loop unmixing (Heslop & Roberts, 2012a), as discussed in section 5.7, are resolved in Figure 8. FORC diagrams provide valuable direct domain state diagnosis based on an interpretive framework provided by extensive experimental evidence from well-characterized samples, theory, numerical simulations, and micromagnetic simulations (Roberts et al., 2014). The use of conventional FORC diagrams for component-specific domain state diagnosis is valuable and is evaluated alongside the FORC-type measurements of Zhao et al. (2017) and FORC-PCA (Harrison et al., 2018), which provide further domain state diagnostic information and unmixing information, respectively, as discussed below.

### 5.9. Remanent, Transient, and Induced FORC Diagrams

The diagnostic value of remFORC, tFORC, and iFORC diagrams (Zhao et al., 2017) is demonstrated for selected Butte Valley samples in Figure 9. Readers are also referred to an extensive characterization with these FORC-type diagrams for Australian soil samples (Hu et al., 2018). As indicated in Figure 6c, Australian soils are dominated magnetically by coarse lithogenic particles. This is reflected in extensive documentation of detrital vortex state and MD particles in tFORC diagrams, along with pedogenic SP/SD particles in remFORC and iFORC diagrams (Hu et al., 2018). Significant high-coercivity hematite



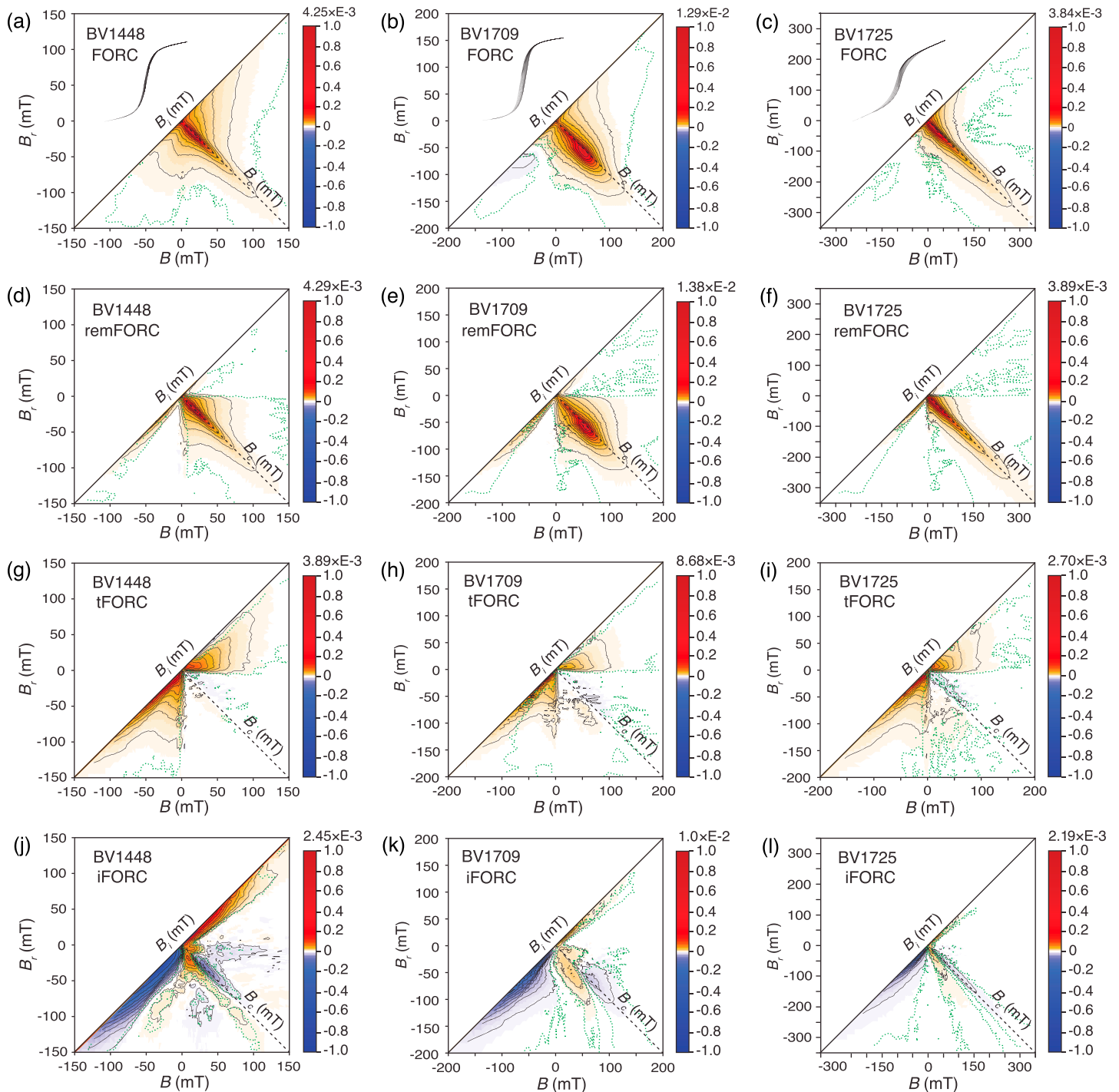


**Figure 9.** Domain state diagnosis for the Butte Valley sediment core (Roberts et al., 1996) using the FORC-type measurements of Zhao et al. (2017). From top to bottom, conventional FORC, remFORC, tFORC, and iFORC diagrams for samples for which conventional FORC diagrams are shown in Figure 8: (a, d, g, and j) BV1448 (dominantly detrital vortex state magnetite), (b, e, h, and k) BV1709 (magnetostatically interacting SD greigite), and (c, f, i, and l) BV1725 (mixture of noninteracting SD and vortex state magnetite and higher-coercivity hematite). See text for discussion. Dashed green contour lines represent the 0.05 significance level determined following Heslop and Roberts (2012b). All samples were measured using an irregular measurement grid (Zhao et al., 2015) with 100-ms averaging time and were processed with SF = 5 for BV1448 and SF = 4 for BV1709 and BV1725.

populations are also evident. Reference to Figures 2b–2e can help readers to understand interpretation of these FORC-type diagrams.

For a dominantly detrital vortex state magnetite sample from Butte Valley (BV1448), a conventional FORC diagram (Figure 9a) is typical of vortex state behavior (Muxworthy & Dunlop, 2002; Roberts et al., 2000, 2017). The remFORC diagram contains evidence of particles near the SP/SD threshold, a noninteracting SD component, and vertical spreading associated with remanence-carrying vortex state particles (Figure 9d). The tFORC diagram is dominated by a vortex signal (Figure 9g) with magnitude close to that of the total FORC signal (Figure 9a). The iFORC diagram contains a dominantly NPN signal due to SD behavior, but it also has a weaker NPN signal due to vortex state behavior at higher  $\{B_i, B_c\}$  values (Figure 9j). A conventional FORC diagram for magnetically interacting SD particles (BV1709; Figure 9b) is typical of greigite (e.g., Roberts et al., 2011). The remFORC diagram indicates the presence of SP and interacting SD particles, which are also typical of greigite (Roberts et al., 2011). The tFORC signature (Figure 9h) is weaker than the conventional FORC and remFORC signals, which indicates that a relatively small part of the particle size distribution extends into the vortex state. As expected, the iFORC diagram has a dominantly NPN signal due to SD behavior (Figure 9k).

A complexly mixed sample (BV1725) with SD and vortex state magnetite and higher-coercivity hematite (Figures 8f and 9c) provides a valuable test of the diagnostic capabilities of the FORC-type diagrams of Zhao et al. (2017). The remFORC diagram indicates a weak component close to the SP/SD threshold, a noninteracting low-coercivity SD response due to magnetite, and a high-coercivity component due to hematite (Figure 9f). The tFORC diagram is indicative of a vortex state magnetite component (Figure 9i), and the iFORC diagram is dominated by a NPN signal due to SD particles (Figure 9l). Overall, this set of FORC-type diagrams provides powerful confirmation of the nature of the mixed magnetic components in sample BV1725.

Conventional FORC diagrams (Pike et al., 1999; Roberts et al., 2000) represent a convolution of remanent, induced, and transient components. Separate assessment of these components using the approach of Zhao et al. (2017) provides diagnostic power in addition to that provided by conventional FORC diagrams. Further development is needed to quantify information about the concentration of each component identified with the approach of Zhao et al. (2017), which will enhance the value of this approach.

### 5.10. FORC Unmixing

FORC unmixing enables magnetic component identification within sample groups. Compared to other unmixing approaches, this is appealing because it provides diagnostic domain state information about constituent magnetic particles and about magnetostatic interactions that is not assessed reliably in other approaches. Harrison et al. (2018) presented several case studies to demonstrate the applicability of the approach, and Roberts, Zhao, et al. (2018) used FORC-PCA to illustrate diagenetic processes in sedimentary environments. These papers provide additional background to the FORC-PCA unmixing example of Butte Valley sediments discussed here (Figure 10). A further example that employed the older FORC-PCA algorithm of Lascu et al. (2015) is provided by Channell et al. (2016).

Individual conventional FORC diagrams for Butte Valley sediments represent mixtures of magnetic minerals with different particle size/domain state distributions (Figure 8). Hysteresis unmixing for Butte Valley samples identified three mixed-EMs (Figure 7) before we identified a central ridge signature due to biogenic magnetite (Roberts et al., 2012), so we adopted a four-component FORC unmixing for these samples using three EMs identified with PCA (Figures 10a–10d) plus a greigite EM (Figure 10e) that is distinct from the other three EMs. A ternary mixing space is defined using two principal components, PC1 and PC2, where measured FORC data fall within a triangle where the three EMs (Figures 10a–10c) are represented by the vertices of the triangle in Figure 10d. EM1 is a high-coercivity ( $>300$  mT), weakly interacting SD hematite with a small SP contribution ( $M_{rs}/M_s = 0.66$  for the extracted FORCs, which is consistent with multiaxial anisotropy in hematite; samples were measured in maximum applied fields of 1 T). EM2 is a lower coercivity, weakly interacting SD magnetite component, with mainly uniaxial features, and a secondary SP/SD peak at the origin, which is responsible for the wasp-waisted extracted FORCs ( $M_{rs}/M_s = 0.385$ ). EM3 is a vortex state magnetite. Contours in Figure 10d represent a zone in which FORC diagrams are physically meaningful; metrics that define these contours (Harrison et al., 2018) guided EM placement. EM2 was placed as far as

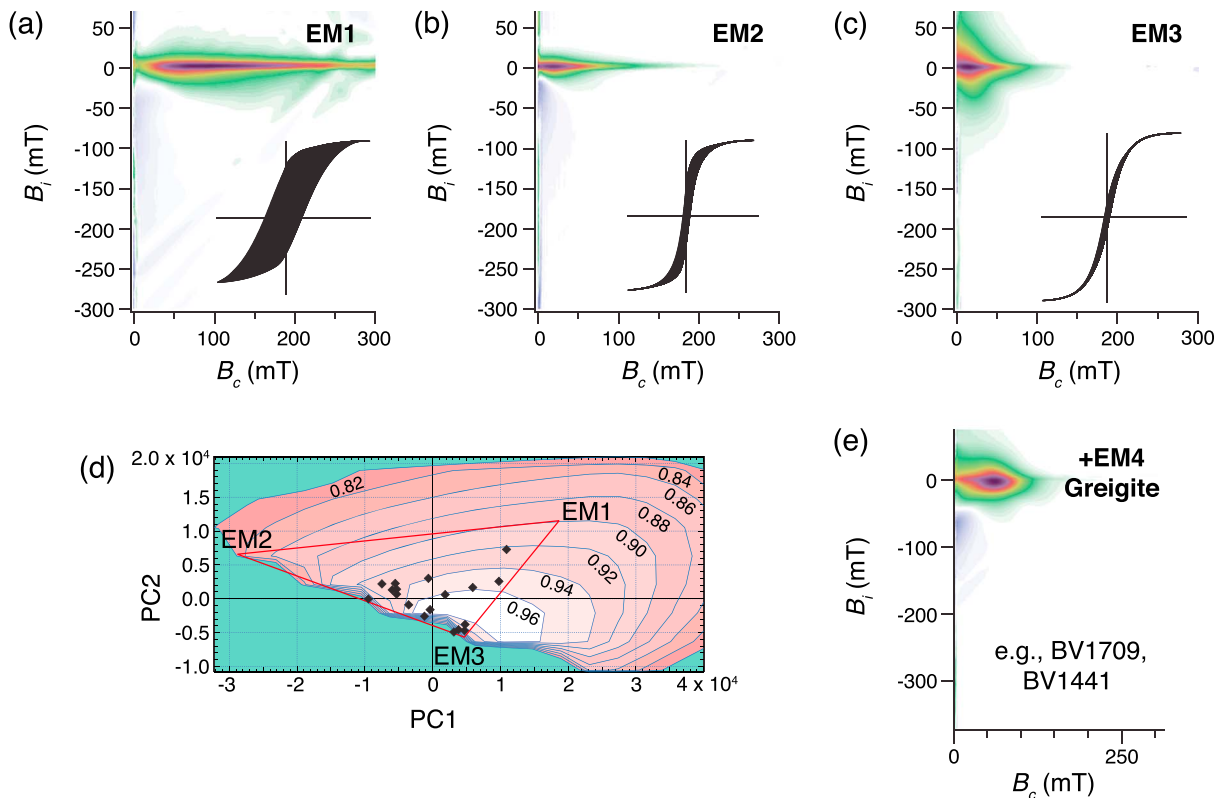


**Figure 10.** Illustration of FORC unmixing of conventional FORC diagrams for the Butte Valley sediment core (Roberts et al., 1996). Three EMs are identified using PCA along with a greigite EM with behavior that is distinct and isolated from that of the other three EMs. FORC diagrams for each EM are as follows (a) high-coercivity ( $>300$  mT), weakly interacting SD hematite with small SP contribution, with mainly uniaxial anisotropy, but with hints of multiaxial anisotropy (EM1) ( $M_{rs}/M_s$  of the extracted FORCs = 0.66, which is consistent with multiaxial anisotropy in hematite); (b) weakly interacting SD magnetite, with mainly uniaxial features (EM2), and a secondary SP/SD peak at the origin, which is responsible for the wasp-waisted extracted FORCs ( $M_{rs}/M_s = 0.385$ ); and (c) vortex state magnetite (EM3). (d) The mixing space is defined using two principal components, PC1 and PC2, where measured FORC data fall within a ternary mixing space with vertices represented by the three EMs in (a–c). The contours in (d) represent the zone in which FORC diagrams are physically meaningful; metrics used to define these contours were used to guide EM placement. EM2 was placed as far as possible from EM3 to remove traces of the vortex state EM3 and to isolate the pure SD EM2 signal. Placement of EM1 is flexible, and interpretation is clear regardless of its exact placement. All samples fall inside the mixing triangle, which makes identification of EM3 straightforward. (e) FORC diagram for the isolated interacting SD greigite component (EM4). VARIFORC smoothing parameters (see Egli, 2013) used in all FORC diagrams are  $s_{c,0} = 5$ ,  $s_{c,1} = 6$ ,  $s_{b,0} = 12$ ,  $s_{b,1} = 12$ , and  $\lambda_c = \lambda_b = 0.1$ , with a correction of 0.0013102 for a vertical offset of the central ridge in EM1 and EM2 due to magnetic viscosity caused by time asymmetry of the FORC measurement (e.g., Pike, Roberts, & Verosub, 2001).

possible from EM3 to remove traces of vortex state EM3 and to isolate the SD EM2. Placement of EM1 is flexible, where the interpretation is clear regardless of its exact position. All samples fall inside the mixing triangle, which makes EM3 identification straightforward. Overall, with FORC unmixing, we identify noninteracting SD magnetite (likely biogenic), noninteracting SD hematite, vortex state magnetite, and a weak SP component (all from the catchment), and interacting SD greigite (authigenic). Signals due to SP rock flour (Heslop & Roberts, 2012a; Roberts et al., 1996) are represented weakly, probably because we selected samples for FORC unmixing from depths in the core where the SP component is not so strong (Figure 7e). Nevertheless, this component is identified clearly in remFORC diagrams (Figures 9d–9f), which have superior diagnosticity with respect to SP components. FORC unmixing has, therefore, identified all of the mineral magnetic components present in the analyzed sample set and with greater diagnostic power than hysteresis unmixing. FORC unmixing can be compromised by several factors, including choice of physically unrealistic or too many end-members, insufficient variability of input data, and artifacts produced by incorrect FORC measurements or processing. Care is needed when using any unmixing method, which is why Harrison et al. (2018) provide feasibility metrics to help users to avoid physically unrealistic solutions. Likewise, ground truthing of FORC unmixing results is critically important for supervising interpretations of FORC results (e.g., Ludwig et al., 2013; Roberts et al., 2012).

## 6. Discussion

### 6.1. Assessment of the Evaluated Approaches for Domain State Diagnosis

Based on the above evaluation of multiple methods used for domain state diagnosis, approaches that enable component-by-component specificity are clearly more suitable for routine use than those based on bulk magnetic parameters. Widespread use of hysteresis parameters in rock magnetism is based on their sensitivity to domain state variations in samples with a single mineral and single grain size, but bulk hysteresis parameters are ambiguous when characterizing complex mixtures that are typical of natural magnetic particle assemblages. This issue is well illustrated by Tauxe et al. (2002) whose micromagnetic simulations of particles with variable anisotropy type, shape, configuration, and domain state fall in different parts of a Néel plot. Addition of other commonly important variables such as cation substitution, interactions, and stress makes the situation more complex. When the response of millions to billions of magnetic particles with distributions of sizes and geometries is summed in geological samples, with potential additional contributions from different minerals with different anisotropy types, it is much less clear how bulk hysteresis parameters provide meaningful information about the domain states of constituent particles. Tauxe et al. (2002) concluded that unambiguous hysteresis interpretation in terms of particle size and shape remains a remote possibility because the same  $M_{rs}$  and  $B_c$  values can be obtained for particles with different size and shape. Complex mixtures appear to be the rule rather than the exception in natural samples, which makes it necessary to identify the magnetic domain state of constituent components to enable meaningful analysis of natural magnetic mineral assemblages.

The above comments encapsulate the detailed arguments of Roberts, Tauxe, et al. (2018) about the lack of domain state diagnosticity of the Day diagram. While the simpler Néel diagram has merits that the Day diagram lacks, as a biplot of bulk hysteresis parameters it does not enable domain state diagnosis on a component-by-component basis for complex samples. The same limitation applies to the Borradaile diagram, although it helpfully avoids the obscuring effects of the  $B_{cr}/B_c$  ratio. The Lascu diagram is designed for use with extensive additional information about constituent magnetic mineral assemblages, but it is still based on bulk parameters. Data for Australian soils and Butte Valley lake sediments are largely indistinguishable in the Lascu diagram (Figure 5c) but are clearly differentiated from each other in Egli diagrams even when the latter is used with bulk instead of component-specific parameters (Figures 6c–6e). The Fabian diagram provides a sensitive measure of SP particle contents and of transient magnetizations associated with vortex state and MD particles. Nevertheless, it provides only a bulk *average* measure of variability rather than component-specific information. We conclude that the Day, Néel, Borradaile, and Fabian diagrams do not provide sufficient domain state diagnosticity for most natural sample sets because of their reliance on bulk hysteresis parameters. The Lascu diagram represents an improved design with incorporation of additional information to provide supervised unmixing, but its use of bulk parameters places it at a disadvantage for domain state diagnosis compared to component-specific approaches. We, therefore, turn our attention to methods that enable domain state identification for constituent magnetic components.

IRM and ARM acquisition/demagnetization curves in their modern form have been a mainstay of mineral magnetic investigations for nearly 20 years. Magnetization curve analyses aim explicitly to identify magnetic components that are related to domain state through coercivity comparison with known materials (e.g., Egli, 2004a, 2004b, 2004c). The principal limitations of these approaches are the nonuniqueness of solutions and selection of appropriate mathematical functions for coercivity distribution fitting. To minimize or avoid nonuniqueness, independent magnetic component identification is needed (e.g., from diagnostic high- or low-temperature data) to provide supervised unmixing (Heslop, 2015). Natural magnetic particle assemblages tend to have skewed particle size/coercivity distributions (Egli, 2003; Heslop et al., 2004; Robertson & France, 1994), yet the simplicity of use of less suitable CLG functions (e.g., Kruiver et al., 2001) has dominated the more appropriate but difficult to fit SGG functions (Egli, 2003). As illustrated by Heslop (2015), CLG functions can require fitting of four components to produce a good match with a measured curve, where only two components are required with SGG functions. We recommend the use of more mathematically appropriate SGG functions, which requires a significant change in user behavior. Among unmixing approaches that involve acquisition/demagnetization curves, the Egli diagram appears to have exceptional domain state specificity. Unfortunately, the experimental demands associated with making measurements with the precision specified by Egli (2004a) has led to this approach not being used as much as it deserves to be.



Given the extent to which hysteresis loops are measured in rock magnetism, it may be surprising that hysteresis unmixing (Heslop & Roberts, 2012a) has yet to be adopted widely. Hysteresis unmixing enables quantification of magnetization components whose contributions can be plotted, for example, throughout a stratigraphic sequence. However, as shown in section 5.7, hysteresis unmixing can suffer from similar nonuniqueness as bulk hysteresis analysis. Nonuniqueness can be addressed using the greater level of information provided by FORC diagrams.

Conventional FORC diagrams are used extensively for domain state diagnosis in rock magnetism. Direct mapping of magnetization reversal signatures makes FORC diagrams highly suitable for routine domain state diagnosis. The examples shown here demonstrate their usefulness, which makes FORC diagrams a leading method for domain state diagnosis. However, the convolution of remanent, induced, and transient magnetizations means that the signals due to some components can obscure those for others in multicomponent mixtures. The additional FORC-type measurements proposed by Zhao et al. (2017) separate these responses to provide markedly improved domain state specificity. Efforts are in progress to quantify the contributions from each component identified with these FORC-type diagrams, which should improve their value significantly. The long measurement time required (about 3 times longer than for conventional FORC measurements) means that they are most likely to be used for a subset of representative samples in any study, but the time investment will provide significant value for understanding the carriers of magnetic signals in natural samples.

FORC unmixing is a valuable approach for unmixing complex samples. It should see increased future use with improvements provided by the algorithm of Harrison et al. (2018). Like all EM unmixing approaches, individual EMs can represent mixtures and the extent to which such mixed EMs can be separated depends on the parsimony of the adopted interpretation and whether the EM represents a naturally produced mixture that cannot be split apart. This limitation is common to unmixing approaches and requires users to maintain a critical eye on unmixing results, but it should not detract from the value of FORC unmixing. Overall, the exceptional single-sample domain state specificity provided by remFORC, tFORC, and iFORC diagrams (Zhao et al., 2017) appears to make this combination of FORC-type diagrams the most suitable of the methods evaluated here for domain state diagnosis.

## 6.2. Limitations of the Evaluated Methods

When evaluating methods for domain state diagnosis in rock magnetism, it is recognized that most methods discussed here bias explicitly toward ferrimagnetic minerals and are generally not designed to assess the often weak imperfect antiferromagnetic components due to hematite and goethite. For example, ARMs are imparted typically with AF demagnetization and DC bias fields that are optimized for acquisition by magnetite and other ferrimagnets and that do not activate high-coercivity hematite and goethite. ARM-based methods, therefore, bias explicitly against high-coercivity mineral detection. FORC analyses are potentially more versatile but often fail to identify hematite over the applied field ranges used. Importantly, hematite is identified using conventional FORC diagrams and remFORC diagrams in this study (e.g., Figures 8f, 9c, 9f, and 10a), which demonstrates that FORC diagrams do not necessarily fail to identify hematite. High-coercivity components can be emphasized by manual adjustment of nonlinear color scales on FORC diagrams (Zhao et al., 2017) and are often indicated by high-coercivity areas over which the FORC distribution remains statistically significant at the 0.05 significance level (cf. Heslop & Roberts, 2012b), as indicated by the green dashed lines in the FORC diagrams in Figure 9.

We suggest a pragmatic solution to the general bias against recognition of higher-coercivity components. The issue of quantifying the relative and absolute concentrations of high-coercivity minerals is a longstanding one in mineral magnetic studies, so additional parameters are generally used to assess high-coercivity components (e.g., S-ratio, HIRM, and L-ratio; Bloemendal et al., 1988; Frank & Nowaczyk, 2008; King & Channell, 1991; Liu et al., 2007; Robinson, 1986). The problem is that the spontaneous magnetization of hematite is  $\sim 200\times$  lower than for magnetite (Dunlop & Özdemir, 1997; O'Reilly, 1984), so that its total content must usually represent  $>90\%$  by mass to be detectable magnetically when magnetite is also present (Frank & Nowaczyk, 2008). This issue is less of a weakness for domain state diagnosis because the weak spontaneous magnetization of hematite and goethite means that the SD to MD transition lies at much larger particle sizes than for ferrimagnetic minerals, so that virtually all hematite and goethite analyzed in natural samples occurs in either the SP or stable SD states. Also, when tightly packed synthetic hematite and



goethite samples are subjected to FORC analyses, they do not interact magnetostatically (e.g., Roberts et al., 2006). This is because, on average, interaction competes with the anisotropy energy, so that when the anisotropy is higher, and magnetization is weaker, as is the case in hematite, interactions have less influence (Muxworthy et al., 2003, 2005). Thus, these minerals almost always occur in noninteracting states so that FORC measurements are also less critical for detecting interactions. A further weakness of most of the methods evaluated here, including FORC diagrams, is that the maximum fields typically applied with standard equipment are far too small to saturate hematite and goethite magnetically. We conclude that the main challenge in rock magnetic studies is to characterize the domain state of the ferrimagnetic mineral fraction because the high-coercivity component of paleomagnetic interest will almost always be in the noninteracting SD state, the contribution of which can be estimated readily using standard parameters designed for this purpose (S-ratio, HIRM, L-ratio, etc.) or using thermal demagnetization of a three-axis IRM (Lowrie, 1990).

As practitioners have known for decades, robust interpretation of a magnetic mineral assemblage requires judicious use of a range of room-, low-, and high-temperature, low- and high-field, and variable frequency techniques. There is no single panacea. Overall, we argue that the diagnostic value of the Day diagram has been overemphasized and we do not recommend its ongoing use. We also do not recommend other approaches that depend on bulk magnetic parameters because component-specific domain state diagnosis is desired. A particular emphasis in environmental magnetism has been the speed and inexpensive nature of bulk magnetic measurements (e.g., Thompson & Oldfield, 1986). Bulk parameters often provide outstanding information about environmental processes. However, domain state diagnosis is particularly important and use of bulk parameters in complex samples does not provide such diagnosis. Thus, diagnostic methods should be used even if it is relatively time-consuming to obtain the necessary measurements. The issues of expense and accessibility of sophisticated methods are real, but few routine magnetic measurement types are genuinely expensive considering that the highest cost involved in research is usually the time of researchers. Time invested in making nondiagnostic measurements is wasted compared to the value of diagnostic measurements. Of course, in high-resolution sediment core studies, for example, it does not make sense to abandon measurement of continuous parameter profiles such as  $\chi$ , ARM, and IRM; supplementing and validating such parameter profiles with domain state-specific determinations for representative samples also makes sense. Domain state diagnosis should rest on secure foundations.

## 7. Conclusions

Our purpose here has been to evaluate the efficacy of various approaches used for domain state diagnosis to help researchers to focus on maximally valuable analyses. We conclude that bulk magnetic parameters tend not to provide sufficient specificity to allow domain state identification in mixed magnetic mineral assemblages that are studied routinely in rock magnetism. We, therefore, do not recommend routine use of the Day, Néel, Borradaile, and Fabian diagrams (Borradaile & Lacroix, 2000; Day et al., 1977; Fabian, 2003; Néel, 1955) unless they are used for pure magnetic mineral components. Reasons for this recommendation are provided by Roberts, Tauxe, et al. (2018), where the focus is on the Day diagram, but most of the same issues also apply to the Néel and Borradaile diagrams. The Lascu diagram (Lascu et al., 2010) is also based on bulk parameters, but it is designed for use with extensive additional mineral magnetic information to constrain interpretation. Nevertheless, compared to component-specific approaches, it can perform ambiguously because of its dependence on bulk parameters.

Several methods are recommended here for routine domain state diagnosis. Unmixing of IRM and ARM acquisition/demagnetization curves is powerful when supervised adequately by additional information to constrain choice from among an infinite number of potential solutions from this type of inversion. Nonuniqueness is a fundamental issue with unmixing (Heslop, 2015), so we stress the importance of obtaining independent information about magnetic mineral components to constrain component selection. The method of Egli (2004a, 2004b, 2004c) stands out among these methods both for its component-by-component specificity and for use of the most suitable mathematical function for component fitting. Nevertheless, the precision required for the time-consuming laboratory measurements associated with this approach, and the complexity of fitting the skewed generalized Gaussian functions recommended by Egli (2003), means that this method has not been adopted as widely as it deserves to be.

Hysteresis loop unmixing (Heslop & Roberts, 2012a) is useful for extracting component-specific information from large hysteresis data sets. Identified end-members can represent mixtures of magnetic components, so independent information is also needed to understand such components. Hysteresis loops for mixed end-members can be affected by the same ambiguities associated with other approaches that employ bulk hysteresis parameters. Thus, as is the case for all end-member unmixing approaches, these limitations must be understood. FORC measurements provide more detailed information, which can generally be used to overcome these limitations.

Conventional FORC diagrams (Pike et al., 1999; Roberts et al., 2000), remFORC, tFORC, and iFORC diagrams (Zhao et al., 2017), and FORC unmixing (Harrison et al., 2018; Lascu et al., 2015) all provide direct information about magnetization reversal, so they are powerful methods for domain state diagnosis. They also provide the additional benefit of approximating interaction field distributions for SD particle assemblages, which is not provided by other methods. Conventional FORC diagrams represent complicated magnetization responses that are deconvolved in remFORC, tFORC, and iFORC diagrams to provide superior domain state diagnosticity. FORC unmixing enables domain state identification for each magnetic component, which is an important advance for understanding complex samples. However, end-members can be mixtures, which must always be borne in mind. Overall, while time-consuming, we conclude that the remFORC, tFORC, and iFORC diagrams of Zhao et al. (2017) provide the most detailed characterization of all domain states present within single magnetically mixed samples.

#### Acknowledgments

We thank Ayako Katayama for her invaluable practical assistance to this work. This work was supported financially by the National Institute of Advanced Industrial Science and Technology, Ministry of Economy, Trade and Industry, Japan (A. P. R., H. O., D. H., X. Z., R. J. H., A. R. M., P. X. H., and T. S.), the Australian Research Council through grant DP160100805 (A. P. R., D. H., R. J. H., A. R. M., and P. X. H.), by the European Research Council under the European Union's Seventh Framework Programme (FP/2007–2013)/ERC grant agreement 320750 (R. J. H.), and by the U.S. National Science Foundation through grants EAR-1547263 and EAR-1827263 (L. T.). The data presented in this paper are largely from Roberts et al. (1996) and Hu et al. (2018).

#### References

- Bloemendal, J., Lamb, B., & King, J. W. (1988). Paleoenvironmental implications of rock-magnetic properties of Late Quaternary sediment cores from the eastern equatorial Atlantic. *Paleoceanography*, 3(1), 61–87. <https://doi.org/10.1029/PA003i001p00061>
- Borradaile, G. J., & Hamilton, T. (2003). Limestones distinguished by magnetic hysteresis in three-dimensional projections. *Geophysical Research Letters*, 30(18), 1973. <https://doi.org/10.1029/2003GL017892>
- Borradaile, G. J., & Lagroix, F. (2000). Magnetic characterization using a three-dimensional hysteresis projection, illustrated with a study of limestones. *Geophysical Journal International*, 141(1), 213–226. <https://doi.org/10.1046/j.1365-246X.2000.00066.x>
- Chang, L., Harrison, R. J., Zeng, F., Berndt, T. A., Roberts, A. P., Heslop, D., & Zhao, X. (2018). Coupled microbial bloom and oxygenation decline recorded by magnetofossils during the Palaeocene-Eocene Thermal Maximum. *Nature Communications*, 9(4007). <https://doi.org/10.1038/s41467-018-06472-y>
- Channell, J. E. T., Harrison, R. J., Lascu, I., McCave, I. N., Hibbert, F. D., & Austin, W. E. N. (2016). Magnetic record of deglaciation using FORC-PCA, sortable-silt grain size, and magnetic excursion at 26 ka, from the Rockall Trough (NE Atlantic). *Geochemistry, Geophysics, Geosystems*, 17, 1823–1841. <https://doi.org/10.1002/2016GC006300>
- Day, R., Fuller, M., & Schmidt, V. A. (1977). Hysteresis properties of titanomagnetites: Grain-size and compositional dependence. *Physics of the Earth and Planetary Interiors*, 13(4), 260–267. [https://doi.org/10.1016/0031-9201\(77\)90108-X](https://doi.org/10.1016/0031-9201(77)90108-X)
- Dunin-Borkowski, R. E., McCartney, M. R., Frankel, R. B., Bazylnski, D. A., Pósfai, M., & Buseck, P. R. (1998). Magnetic microstructure of magnetotactic bacteria by electron holography. *Science*, 282(5395), 1868–1870. <https://doi.org/10.1126/science.282.5395.1868>
- Dunlop, D. J. (1986). Hysteresis properties of magnetite and their dependence on particle size: A test of pseudo-single-domain remanence models. *Journal of Geophysical Research*, 91(B9), 9569–9584. <https://doi.org/10.1029/JB091iB09p09569>
- Dunlop, D. J. (2002). Theory and application of the Day plot ( $M_{rs}/M_s$  versus  $H_{cr}/H_c$ ): 1. Theoretical curves and tests using titanomagnetite data. *Journal of Geophysical Research*, 107(B3), 2056. <https://doi.org/10.1029/2001JB000486>
- Dunlop, D. J., & Argyle, K. S. (1997). Thermoremanence, anhysteretic remanence and susceptibility of submicron magnetites: Nonlinear field dependence and variation with grain size. *Journal of Geophysical Research*, 102(B9), 20,199–20,210. <https://doi.org/10.1029/97JB00957>
- Dunlop, D. J., & Özdemir, Ö. (1997). *Rock magnetism: Fundamentals and frontiers* (p. 573). Cambridge: Cambridge University Press. <https://doi.org/10.1017/CBO9780511612794>
- Egli, R. (2003). Analysis of the field dependence of remanent magnetization curves. *Journal of Geophysical Research*, 108(B2), 2081. <https://doi.org/10.1029/2002JB002023>
- Egli, R. (2004a). Characterization of individual rock magnetic components by analysis of remanence curves: 1. Unmixing natural sediments. *Studia Geophysica et Geodaetica*, 48(2), 391–446. <https://doi.org/10.1023/B:SGEG.0000020839.45304.6d>
- Egli, R. (2004b). Characterization of individual rock magnetic components by analysis of remanence curves: 2. Fundamental properties of coercivity distributions. *Physics and Chemistry of the Earth*, 29(13–14), 851–867. <https://doi.org/10.1016/j.pce.2004.04.001>
- Egli, R. (2004c). Characterization of individual rock magnetic components by analysis of remanence curves: 3. Bacterial magnetite and natural processes in lakes. *Physics and Chemistry of the Earth*, 29(13–14), 869–884. <https://doi.org/10.1016/j.pce.2004.03.010>
- Egli, R. (2013). VARIFORC: An optimized protocol for calculating non-regular first-order reversal curve (FORC) diagrams. *Global and Planetary Change*, 110(C), 302–320. <https://doi.org/10.1016/j.gloplacha.2013.08.003>
- Egli, R., Chen, A. P., Winklhofer, M., Kodama, K. P., & Horng, C. S. (2010). Detection of noninteracting single domain particles using first-order reversal curve diagrams. *Geochemistry, Geophysics, Geosystems*, 11, Q01Z11. <https://doi.org/10.1029/2009GC002916>
- Egli, R., & Lowrie, W. (2002). Anhysteretic remanent magnetization of fine magnetic particles. *Journal of Geophysical Research*, 107(B10), 2209. <https://doi.org/10.1029/2001JB000671>
- Egli, R., & Winklhofer, M. (2014). Recent developments on processing and interpretation aspects of first-order reversal curves (FORC). *Scientific Proceedings of Kazan Federal University*, 156(1), 14–53.
- Evans, M. E., Krása, D., Williams, W., & Winklhofer, M. (2006). Magnetostatic interactions in a natural magnetite-ulvospinel system. *Journal of Geophysical Research*, 111, B12S16. <https://doi.org/10.1029/2006JB004454>

- Fabian, K. (2003). Some additional parameters to estimate domain state from isothermal remanent magnetization. *Earth and Planetary Science Letters*, 213(3–4), 337–345. [https://doi.org/10.1016/S0012-821X\(03\)00329-7](https://doi.org/10.1016/S0012-821X(03)00329-7)
- Fabian, K., & von Dobeneck, T. (1997). Isothermal magnetization of samples with stable Preisach function: A survey of hysteresis, remanence, and rock magnetic parameters. *Journal of Geophysical Research*, 102(B8), 17,659–17,677. <https://doi.org/10.1029/97JB01051>
- Frank, U., & Nowaczyk, N. R. (2008). Mineral magnetic properties of artificial samples systematically mixed from haematite and magnetite. *Geophysical Journal International*, 175(2), 449–461. <https://doi.org/10.1111/j.1365-246X.2008.03821.x>
- Harrison, R. J. (2009). Magnetic ordering in the ilmenite-hematite solid solution: A computational study of the low-temperature spin glass region. *Geochemistry, Geophysics, Geosystems*, 10, Q02Z02. <https://doi.org/10.1029/2008GC002240>
- Harrison, R. J., Dunin-Borkowski, R. E., & Putnis, A. (2002). Direct imaging of nanoscale magnetic interactions in minerals. *Proceedings of the National Academy of Sciences of the United States of America*, 99(26), 16,556–16,561. <https://doi.org/10.1073/pnas.262514499>
- Harrison, R. J., & Feinberg, J. M. (2008). FORCinel: An improved algorithm for calculating first-order reversal curve distributions using locally weighted regression smoothing. *Geochemistry, Geophysics, Geosystems*, 9, Q05016. <https://doi.org/10.1029/2008GC001987>
- Harrison, R. J., & Lascu, I. (2014). FORCulator: A micromagnetic tool for simulating first-order reversal curve diagrams. *Geochemistry, Geophysics, Geosystems*, 15, 4671–4691. <https://doi.org/10.1002/2014GC005582>
- Harrison, R. J., Muraszko, J., Heslop, D., Lascu, I., Muxworthy, A. R., & Roberts, A. P. (2018). An improved algorithm for unmixing first-order reversal curve diagrams using principal component analysis. *Geochemistry, Geophysics, Geosystems*, 19, 1595–1610. <https://doi.org/10.1029/2018GC007511>
- Heider, F., Zitzelsberger, A., & Fabian, K. (1996). Magnetic susceptibility and remanent coercive force in grown magnetite crystals from 0.1  $\mu\text{m}$  to 6 mm. *Physics of the Earth and Planetary Interiors*, 93(3–4), 239–256. [https://doi.org/10.1016/0031-9201\(95\)03071-9](https://doi.org/10.1016/0031-9201(95)03071-9)
- Heslop, D. (2015). Numerical strategies for magnetic mineral unmixing. *Earth-Science Reviews*, 150, 256–284. <https://doi.org/10.1016/j.earscirev.2015.07.007>
- Heslop, D., Dekkers, M. J., Kruiver, P. P., & van Oorschot, I. H. M. (2002). Analysis of isothermal remanent magnetization acquisition curves using the expectation-maximization algorithm. *Geophysical Journal International*, 148(1), 58–64. <https://doi.org/10.1046/j.0956-540x.2001.01558.x>
- Heslop, D., McIntosh, G., & Dekkers, M. J. (2004). Using time- and temperature-dependent Preisach models to investigate the limitations of modelling isothermal remanent magnetization acquisition curves with cumulative log Gaussian functions. *Geophysical Journal International*, 157(1), 55–63. <https://doi.org/10.1111/j.1365-246X.2004.02155.x>
- Heslop, D., & Roberts, A. P. (2012a). A method for unmixing magnetic hysteresis loops. *Journal of Geophysical Research*, 117, B03103. <https://doi.org/10.1029/2011JB008859>
- Heslop, D., & Roberts, A. P. (2012b). Estimation of significance levels and confidence intervals for first-order reversal curve distributions. *Geochemistry, Geophysics, Geosystems*, 13, Q12Z40. <https://doi.org/10.1029/2012GC004115>
- Heslop, D., Roberts, A. P., & Chang, L. (2014). Characterizing magnetofossils from first-order reversal curve (FORC) central ridge signatures. *Geochemistry, Geophysics, Geosystems*, 15, 2170–2179. <https://doi.org/10.1002/2014GC005291>
- Hu, P. X., Zhao, X., Roberts, A. P., Heslop, D., & Viscarra Rossel, R. A. (2018). Magnetic domain state diagnosis in soils, loess, and marine sediments from multiple first-order reversal curve (FORC)-type diagrams. *Journal of Geophysical Research: Solid Earth*, 123, 998–1017. <https://doi.org/10.1002/2017JB015195>
- Hunt, C., Moskowitz, B. M., & Banerjee, S. K. (1995). Magnetic properties of rocks and minerals. In T. J. Ahrens (Ed.), *Rock physics & phase relations: Handbook of physical constants* (Vol. 3, pp. 189–204). Washington, DC: American Geophysical Union. <https://doi.org/10.1029/RF003p0189>
- Ishikawa, Y., Saito, N., Arai, M., Watanabe, Y., & Takei, H. (1985). A new oxide spin glass system of  $(1-x)\text{FeTiO}_3-x\text{Fe}_2\text{O}_3$ : I. Magnetic properties. *Journal of the Physical Society of Japan*, 54(1), 312–325. <https://doi.org/10.1143/JPSJ.54.312>
- Jackson, M. (1990). Diagenetic sources of stable remanence in remagnetized Paleozoic cratonic carbonates: A rock magnetic study. *Journal of Geophysical Research*, 95(B3), 2753–2761. <https://doi.org/10.1029/JB095iB03p02753>
- Jackson, M., & Solheid, P. (2010). On the quantitative analysis and evaluation of magnetic hysteresis data. *Geochemistry, Geophysics, Geosystems*, 11, Q04Z15. <https://doi.org/10.1029/2009GC002932>
- Jackson, M., Worm, H.-U., & Banerjee, S. K. (1990). Fourier analysis of digital hysteresis data: Rock magnetic applications. *Physics of the Earth and Planetary Interiors*, 65(1–2), 78–87. [https://doi.org/10.1016/0031-9201\(90\)90077-B](https://doi.org/10.1016/0031-9201(90)90077-B)
- Joffe, I., & Heuberger, R. (1974). Hysteresis properties of distributions of cubic single-domain ferromagnetic particles. *Philosophical Magazine*, 29(5), 1051–1059. <https://doi.org/10.1080/14786437408226590>
- Johnson, H. P., Lowrie, W., & Kent, D. V. (1975). Stability of anhysteretic remanent magnetization in fine and coarse magnetite and maghemite particles. *Geophysical Journal of the Royal Astronomical Society*, 41(1), 1–10. <https://doi.org/10.1111/j.1365-246X.1975.tb05480.x>
- King, J. W., & Channell, J. E. T. (1991). Sedimentary magnetism, environmental magnetism, and magnetostratigraphy. *Reviews of Geophysics*, 29(S1), 358–370. <https://doi.org/10.1002/rog.1991.29.s1.358>
- Kruiver, P. P., Dekkers, M. J., & Heslop, D. (2001). Quantification of magnetic coercivity components by the analysis of acquisition curves of isothermal remanent magnetization. *Earth and Planetary Science Letters*, 189(3–4), 269–276. [https://doi.org/10.1016/S0012-821X\(01\)00367-3](https://doi.org/10.1016/S0012-821X(01)00367-3)
- Larrasoana, J. C., Roberts, A. P., Musgrave, R. J., Gràcia, E., Piñero, E., Vega, M., & Martínez-Ruiz, F. (2007). Diagenetic formation of greigite and pyrrhotite in marine sedimentary systems containing gas hydrates. *Earth and Planetary Science Letters*, 261(3–4), 350–366. <https://doi.org/10.1016/j.epsl.2007.06.032>
- Lascu, I., Banerjee, S. K., & Berquó, T. S. (2010). Quantifying the concentration of ferrimagnetic particles in sediments using rock magnetic methods. *Geochemistry, Geophysics, Geosystems*, 11, Q08Z19. <https://doi.org/10.1029/2010GC003182>
- Lascu, I., Einsle, J. F., Ball, M. R., & Harrison, R. J. (2018). The vortex state in geologic materials: A micromagnetic perspective. *Journal of Geophysical Research: Solid Earth*, 123, 7285–7304. <https://doi.org/10.1029/2018JB015909>
- Lascu, I., Harrison, R. J., Li, Y. T., Muraszko, J. R., Channell, J. E. T., Piotrowski, A. M., & Hodell, D. A. (2015). Magnetic unmixing of first-order reversal curve diagrams using principal component analysis. *Geochemistry, Geophysics, Geosystems*, 16, 2900–2915. <https://doi.org/10.1002/2015GC005909>
- Liu, Q. S., Roberts, A. P., Torrent, J., Horng, C. S., & Larrasoana, J. C. (2007). What do the HIRM and S-ratio really measure in environmental magnetism? *Geochemistry, Geophysics, Geosystems*, 8, Q09011. <https://doi.org/10.1029/2007GC001717>
- Lowrie, W. (1990). Identification of ferromagnetic minerals in a rock by coercivity and unblocking temperature properties. *Geophysical Research Letters*, 17(2), 159–162. <https://doi.org/10.1029/GL017i002p00159>

- Lowrie, W., & Fuller, M. (1971). On the alternating field demagnetization characteristics of multidomain thermoremanent magnetization in magnetite. *Journal of Geophysical Research*, 76(26), 6339–6349. <https://doi.org/10.1029/JB076i026p06339>
- Ludwig, P., Egli, R., Bishop, S., Chernenko, V., Frederichs, T., Rugel, G., et al. (2013). Characterization of primary and secondary magnetite in marine sediment by combining chemical and magnetic unmixing techniques. *Global and Planetary Change*, 110, 321–339. <https://doi.org/10.1016/j.gloplacha.2013.08.018>
- Maher, B. A. (1988). Magnetic properties of some synthetic sub-micron magnetites. *Geophysical Journal*, 94(1), 83–96. <https://doi.org/10.1111/j.1365-246X.1988.tb03429.x>
- Maxbauer, D. P., Feinberg, J. M., & Fox, D. L. (2016). MAX UnMix: A web application for unmixing magnetic coercivity distributions. *Computers & Geosciences*, 95, 140–145. <https://doi.org/10.1016/j.cageo.2016.07.009>
- Mayergoyz, I. D. (1986). Mathematical models of hysteresis. *IEEE Transactions on Magnetism*, MAG, 22(5), 603–608. <https://doi.org/10.1109/TMAG.1986.1064347>
- Muxworthy, A. R., & Dunlop, D. J. (2002). First-order reversal curve (FORC) diagrams for pseudo-single-domain magnetites at high temperature. *Earth and Planetary Science Letters*, 203(1), 369–382. [https://doi.org/10.1016/S0012-821X\(02\)00880-4](https://doi.org/10.1016/S0012-821X(02)00880-4)
- Muxworthy, A. R., King, J. G., & Heslop, D. (2005). Assessing the ability of first-order reversal curve (FORC) diagrams to unravel complex magnetic signals. *Journal of Geophysical Research*, 110, B01105. <https://doi.org/10.1029/2004JB003195>
- Muxworthy, A. R., Williams, W., & Virdee, D. (2003). Effect of magnetostatic interactions on the hysteresis parameters of single-domain and pseudo-single-domain grains. *Journal of Geophysical Research*, 108(B11), 2517. <https://doi.org/10.1029/2003JB002588>
- Nagata, T. (1961). *Rock magnetism* (p. 366). Tokyo: Maruzen.
- Néel, L. (1954). Remarques sur la théorie des propriétés magnétiques des substances dures. *Applied Scientific Research*, B, 4(1), 13–24. <https://doi.org/10.1007/BF02316465>
- Néel, L. (1955). Some theoretical aspects of rock-magnetism. *Advances in Physics*, 4(14), 191–243. <https://doi.org/10.1080/00018735500101204>
- Newell, A. J., & Merrill, R. T. (2000). Nucleation and stability of ferromagnetic states. *Journal of Geophysical Research*, 105(B8), 19,377–19,391. <https://doi.org/10.1029/2000JB900121>
- O'Reilly, W. (1984). *Rock and mineral magnetism* (p. 220). Glasgow: Blackie and Son. <https://doi.org/10.1007/978-1-4684-8468-7>
- Pike, C., & Fernandez, A. (1999). An investigation of magnetic reversal in submicron-scale Co dots using first order reversal curve diagrams. *Journal of Applied Physics*, 85(9), 6668–6676. <https://doi.org/10.1063/1.370177>
- Pike, C. R., Roberts, A. P., Dekkers, M. J., & Verosub, K. L. (2001). An investigation of multi-domain hysteresis mechanisms using FORC diagrams. *Physics of the Earth and Planetary Interiors*, 126(1–2), 11–25. [https://doi.org/10.1016/S0031-9201\(01\)00241-2](https://doi.org/10.1016/S0031-9201(01)00241-2)
- Pike, C. R., Roberts, A. P., & Verosub, K. L. (1999). Characterizing interactions in fine magnetic particle systems using first order reversal curves. *Journal of Applied Physics*, 85(9), 6660–6667. <https://doi.org/10.1063/1.370176>
- Pike, C. R., Roberts, A. P., & Verosub, K. L. (2001). First-order reversal curve diagrams and thermal relaxation effects in magnetic particles. *Geophysical Journal International*, 145(3), 721–730. <https://doi.org/10.1046/j.0956-540x.2001.01419.x>
- Preisach, F. (1935). Über die magnetische Nachwirkung. *Zeitschrift für Physik*, 94(5–6), 277–302. <https://doi.org/10.1007/BF01349418>
- Radhakrishnamurty, C., Likhite, S. D., Deutsch, E. R., & Murthy, G. S. (1981). A comparison of the magnetic properties of synthetic titanomagnetites and basalts. *Physics of the Earth and Planetary Interiors*, 26(1–2), 37–46. [https://doi.org/10.1016/0031-9201\(81\)90095-9](https://doi.org/10.1016/0031-9201(81)90095-9)
- Roberts, A. P., Almeida, T. P., Church, N. S., Harrison, R. J., Heslop, D., Li, Y., et al. (2017). Resolving the origin of pseudo-single domain magnetic behavior. *Journal of Geophysical Research: Solid Earth*, 122, 9534–9558. <https://doi.org/10.1002/2017JB014860>
- Roberts, A. P., Chang, L., Heslop, D., Florindo, F., & Larrasoana, J. C. (2012). Searching for single domain magnetite in the “pseudo-single-domain” sedimentary haystack: Implications of biogenic magnetite preservation for sediment magnetism and relative paleointensity determinations. *Journal of Geophysical Research*, 117, B08104. <https://doi.org/10.1029/2012JB009412>
- Roberts, A. P., Chang, L., Rowan, C. J., Horng, C. S., & Florindo, F. (2011). Magnetic characteristics of sedimentary greigite (Fe<sub>3</sub>S<sub>4</sub>): An update. *Reviews of Geophysics*, 49, RG1002. <https://doi.org/10.1029/2010RG000336>
- Roberts, A. P., Cui, Y. L., & Verosub, K. L. (1995). Wasp-waisted hysteresis loops: Mineral magnetic characteristics and discrimination of components in mixed magnetic systems. *Journal of Geophysical Research*, 100(B9), 17,909–17,924. <https://doi.org/10.1029/95JB00672>
- Roberts, A. P., Heslop, D., Zhao, X., & Pike, C. R. (2014). Understanding fine magnetic particle systems through use of first-order reversal curve diagrams. *Reviews of Geophysics*, 52, 557–602. <https://doi.org/10.1002/2014RG000462>
- Roberts, A. P., Liu, Q. S., Rowan, C. J., Chang, L., Carvallo, C., Torrent, J., & Horng, C. S. (2006). Characterization of hematite ( $\alpha$ -Fe<sub>2</sub>O<sub>3</sub>), goethite ( $\alpha$ -FeOOH), greigite (Fe<sub>3</sub>S<sub>4</sub>), and pyrrhotite (Fe<sub>7</sub>S<sub>8</sub>) using first-order reversal curve diagrams. *Journal of Geophysical Research*, 111, B12S35. <https://doi.org/10.1029/2006JB004715>
- Roberts, A. P., Pike, C. R., & Verosub, K. L. (2000). First-order reversal curve diagrams: A new tool for characterizing the magnetic properties of natural samples. *Journal of Geophysical Research*, 105(B12), 28,461–28,475. <https://doi.org/10.1029/2000JB900326>
- Roberts, A. P., Reynolds, R. L., Verosub, K. L., & Adam, D. P. (1996). Environmental magnetic implications of greigite (Fe<sub>3</sub>S<sub>4</sub>) formation in a 3 m.y. lake sediment record from Butte Valley, northern California. *Geophysical Research Letters*, 23(20), 2859–2862. <https://doi.org/10.1029/96GL02831>
- Roberts, A. P., Sagnotti, L., Florindo, F., Bohaty, S. M., Verosub, K. L., Wilson, G. S., & Zachos, J. C. (2013). Environmental magnetic record of paleoclimate, unroofing of the Transantarctic Mountains, and volcanism in late Eocene to early Miocene glaci-marine sediments from the Victoria Land Basin, Ross Sea, Antarctica. *Journal of Geophysical Research: Solid Earth*, 118, 1845–1861. <https://doi.org/10.1002/jgrb.50151>
- Roberts, A. P., Tauxe, L., Heslop, D., Zhao, X., & Jiang, Z. X. (2018). A critical appraisal of the “Day” diagram. *Journal of Geophysical Research: Solid Earth*, 123, 2618–2644. <https://doi.org/10.1002/2017JB015247>
- Roberts, A. P., Zhao, X., Harrison, R. J., Heslop, D., Muxworthy, A. R., Rowan, C. J., et al. (2018). Signatures of reductive magnetic mineral diagenesis from unmixing of first-order reversal curves. *Journal of Geophysical Research: Solid Earth*, 123, 4500–4522. <https://doi.org/10.1002/2018JB015706>
- Robertson, D. J., & France, D. E. (1994). Discrimination of remanence-carrying minerals in mixtures, using isothermal remanent magnetization acquisition curves. *Physics of the Earth and Planetary Interiors*, 82(3–4), 223–234. [https://doi.org/10.1016/0031-9201\(94\)90074-4](https://doi.org/10.1016/0031-9201(94)90074-4)
- Robinson, P., Harrison, R. J., McEnroe, S. A., & Hargraves, R. B. (2002). Lamellar magnetism in the haematite-ilmenite series as an explanation for strong remanent magnetization. *Nature*, 418, 517–520. <https://doi.org/10.1038/nature00942>
- Robinson, S. G. (1986). The late Pleistocene palaeoclimatic record of North Atlantic deep-sea sediments revealed by mineral-magnetic measurements. *Physics of the Earth and Planetary Interiors*, 42(1–2), 22–47. [https://doi.org/10.1016/S0031-9201\(86\)80006-1](https://doi.org/10.1016/S0031-9201(86)80006-1)



- Schabes, M. E., & Bertram, H. N. (1988). Magnetization processes in ferromagnetic cubes. *Journal of Applied Physics*, 64(3), 1347–1357. <https://doi.org/10.1063/1.341858>
- Scheidt, S., Egli, R., Frederichs, T., Hambach, U., & Rolf, C. (2017). A mineral magnetic characterization of the Plio-Pleistocene fluvial infill of the Heidelberg Basin (Germany). *Geophysical Journal International*, 210(2), 743–764. <https://doi.org/10.1093/gji/ggx154>
- Stoner, E. C., & Wohlfarth, E. P. (1948). A mechanism of magnetic hysteresis in heterogeneous alloys. *Philosophical Transactions of the Royal Society of London*, 240(826), 599–642. <https://doi.org/10.1098/rsta.1948.0007>
- Tauxe, L., Bertram, H. N., & Seberino, C. (2002). Physical interpretation of hysteresis loops: Micromagnetic modeling of fine particle magnetite. *Geochemistry, Geophysics, Geosystems*, 3(10), 1055. <https://doi.org/10.1029/2001GC000241>
- Tauxe, L., Mullender, T. A. T., & Pick, T. (1996). Potbellies, wasp-waists, and superparamagnetism in magnetic hysteresis. *Journal of Geophysical Research*, 101(B1), 571–583. <https://doi.org/10.1029/95JB03041>
- Thompson, R., & Oldfield, F. (1986). *Environmental magnetism* (p. 228). Winchester, MA: Allen and Unwin. <https://doi.org/10.1007/978-94-011-8036-8>
- Walker, M., Mayo, P. I., O'Grady, K., Charles, S. W., & Chantrell, R. W. (1993). The magnetic properties of single-domain particles with cubic anisotropy: 1. Hysteresis loops. *Journal of Physics: Condensed Matter*, 5(17), 2779–2792. <https://doi.org/10.1088/0953-8984/5/17/012>
- Wang, D., & van der Voo, R. (2004). The hysteresis properties of multidomain magnetite and titanomagnetite/titanomaghemite in mid-ocean ridge basalts. *Earth and Planetary Science Letters*, 220(1–2), 175–184. [https://doi.org/10.1016/S0012-821X\(04\)00052-4](https://doi.org/10.1016/S0012-821X(04)00052-4)
- Williams, W., & Dunlop, D. J. (1989). Three-dimensional micromagnetic modelling of ferromagnetic domain structure. *Nature*, 337(6208), 634–637. <https://doi.org/10.1038/337634a0>
- Williams, W., & Dunlop, D. J. (1995). Simulation of magnetic hysteresis in pseudo-single-domain grains of magnetite. *Journal of Geophysical Research*, 100(B3), 3859–3871. <https://doi.org/10.1029/94JB02878>
- Williams, W., Evans, M. E., & Krása, D. (2010). Micromagnetics of paleomagnetically significant mineral grains with complex morphology. *Geochemistry, Geophysics, Geosystems*, 11, Q02Z14. <https://doi.org/10.1029/2009GC002828>
- Williams, W., Muxworthy, A. R., & Evans, M. E. (2011). A micromagnetic investigation of magnetite grains in the form of Platonic polyhedra with surface roughness. *Geochemistry, Geophysics, Geosystems*, 12, Q10Z31. <https://doi.org/10.1029/2011gc003560>
- Yu, Y., & Tauxe, L. (2005). On the use of magnetic transient hysteresis in paleomagnetism for granulometry. *Geochemistry, Geophysics, Geosystems*, 6, Q01H14. <https://doi.org/10.1029/2004GC000839>
- Zhao, X., Heslop, D., & Roberts, A. P. (2015). A protocol for variable-resolution first-order reversal curve measurements. *Geochemistry, Geophysics, Geosystems*, 16, 1364–1377. <https://doi.org/10.1002/2014GC005680>
- Zhao, X., Roberts, A. P., Heslop, D., Paterson, G. A., Li, Y. L., & Li, J. H. (2017). Magnetic domain state diagnosis using hysteresis reversal curves. *Journal of Geophysical Research: Solid Earth*, 122, 4767–4789. <https://doi.org/10.1002/2016JB013683>